**Geoscientific
Model Development**

MADE-in: a new aerosol microphysics submodel for global simulation of insoluble particles and their mixing state

V. Aquila[1,*], **J. Hendricks**[1], **A. Lauer**[2], **N. Riemer**[3], **H. Vogel**[4], **D. Baumgardner**[5], **A. Minikin**[1], **A. Petzold**[1],
J. P. Schwarz[6], **J. R. Spackman**[6], **B. Weinzierl**[1], **M. Righi**[1], and **M. Dall'Amico**[1,**]

[1]Deutsches Zentrum für Luft- und Raumfahrt (DLR), Institut für Physik der Atmosphäre, Oberpfaffenhofen, Germany
[2]International Pacific Research Center, University of Hawaii, Honolulu, Hawaii, USA
[3]Department of Atmospheric Sciences, University of Illinois at Urbana-Champaign, Urbana, Illinois, USA
[4]Institut für Meteorologie und Klimaforschung, Karlsruhe Institute of Technology, Eggenstein-Leopoldshafen, Germany
[5]Centro de Ciencias de la Atmosfera, Universidad Nacional Autonoma de Mexico, Mexico City, Mexico
[6]Chemical Sciences Division, Earth System Research Laboratory, NOAA, Boulder, Colorado, USA
*now at: NASA Goddard Space Flight Center, Greenbelt, Maryland, USA
**now at: Astrium GmbH, Ottobrunn, Germany

Abstract. Black carbon (BC) and mineral dust are among the most abundant insoluble aerosol components in the atmosphere. When released, most BC and dust particles are externally mixed with other aerosol species. Through coagulation with particles containing soluble material and condensation of gases, the externally mixed particles may obtain a liquid coating and be transferred into an internal mixture. The mixing state of BC and dust aerosol particles influences their radiative and hygroscopic properties, as well as their ability of forming ice crystals.

We introduce the new aerosol microphysics submodel MADE-in, implemented within the ECHAM/MESSy Atmospheric Chemistry global model (EMAC). MADE-in is able to track mass and number concentrations of BC and dust particles in their different mixing states, as well as particles free of BC and dust. MADE-in describes these three classes of particles through a superposition of seven log-normally distributed modes, and predicts the evolution of their size distribution and chemical composition. Six out of the seven modes are mutually interacting, allowing for the transfer of mass and number among them. Separate modes for the different mixing states of BC and dust particles in EMAC/MADE-in allow for explicit simulations of the relevant aging processes, i.e. condensation, coagulation and cloud process-
ing. EMAC/MADE-in has been evaluated with surface and airborne measurements and mostly performs well both in the planetary boundary layer and in the upper troposphere and lowermost stratosphere.

1 Introduction

Atmospheric aerosol is of primary importance in the climate system (e.g., Forster et al., 2007). Its effect on climate is both direct (e.g., Haywood and Boucher, 2000), via scattering and absorption of radiation, and indirect, by inducing changes in cloud properties (e.g., Lohmann and Feichter, 2005). Modeling the climate effect of aerosol is a very challenging problem, since it depends not only on the mass of each aerosol species, but also on the number of particles, their size and their mixing state (Ghan and Schwartz, 2007). These parameters influence the radiative properties of aerosols as well as their ability to interact with clouds.

The main components of atmospheric aerosol are sulfate, ammonium, nitrate, sea salt, carbonaceous material, both as black and organic carbon, and mineral dust. Some of these components are water insoluble, particularly black carbon, the major mineral dust compounds, as well as an uncertain fraction of organic carbon. Insoluble components can affect the hygroscopicity of aerosols. This can have effects on their interactions with clouds (e.g. McFiggans et al., 2006) as well

as their radiative properties (e.g. Jacobson, 2000). Here, we aim at an improved representation of insoluble particles in a global aerosol-climate model, with a particular focus on particles containing black carbon (BC) or mineral dust.

BC and dust particles can be either externally mixed with other aerosol species, i.e. bare BC or dust particles coexist with other aerosols, or internally mixed, i.e. a particle contains BC and/or dust mixed with other species. An internally mixed particle could, for instance, consist of an insoluble core of BC or dust coated with soluble material. Freshly emitted BC and mineral dust particles are mainly externally mixed, but condensation of trace gases and coagulation with soluble particles may transfer them to an internal mixture (Kotzick and Niessner, 1999; Weingartner et al., 1997, 2000; Okada et al., 2005; Song et al., 2005; Moteki et al., 2007; Sullivan et al., 2007). This aging process may allow initially insoluble aerosols to be activated to form cloud droplets (Kelly et al., 2007; Khalizov et al., 2009; Sullivan et al., 2009). This implies that internally mixed insoluble particles may be more efficiently removed by precipitation than externally mixed ones (Hitzenberger et al., 2001; Zuberi et al., 2005).

The mixing state of insoluble particles can also have other important effects. Several experimental and theoretical studies showed that the presence of a soluble coating changes the ability of BC to absorb solar radiation (Jacobson, 2000, 2001a; Schnaiter et al., 2005; Bond et al., 2006; Shiraiwa et al., 2008; Naoe et al., 2009). Others focused on the potential of BC and dust particles to act as ice nuclei (IN): DeMott et al. (1999) concluded that a soluble coating may enhance the ability of BC to act as IN in cirrus, while Möhler et al. (2005) found that it may decrease the particles' ice nucleation efficiency. Also the ability of dust particles to initiate heterogeneous nucleation of ice crystals under cirrus conditions might be reduced due to soluble coatings (e.g. Möhler et al., 2008; Cziczo et al., 2009; Koehler et al., 2010). It was also shown that soluble coatings may have an effect on the heterogeneous freezing ability of mineral dust in the mixed-phase cloud regime (Chernoff and Bertram, 2010; Niedermeier et al., 2010). Global simulations by Hoose et al. (2008) and Lohmann and Hoose (2009) demonstrated that the deactivation of ice nuclei due to soluble coatings and the resulting effects on mixed-phase clouds may have relevant climate effects.

Hence, in order to refine model assessments of the role of BC and mineral dust in the global climate system, it is necessary to simulate not only their mass concentration, but also their number concentration, size distribution, and, importantly, their mixing state. The first methods to simulate the number concentration and size distribution of aerosol particles in larger-scale atmospheric models were initially developed and applied within regional models, as, for instance, the Regional Particulate Model (RPM) (Binkowski and Shankar, 1995) and the European Air pollution Dispersion model (EURAD) coupled to the two-moment Modal Aerosol Dynamics model for Europe (MADE) (Ackermann et al., 1998),

both applying a modal representation of the aerosol size distribution (Whitby and McMurry, 1997). These methods, however, were computationally too expensive for applications in global climate models. With the increase in computer processing capacities, more detailed aerosol schemes were also applied on the global scale. For instance, Adams and Seinfeld (2002) incorporated the TwO-Moment Aerosol Sectional (TOMAS) model in the GISS GCM II-prime global model to simulate also the number concentration and the microphysics of sulfate aerosols. Lauer et al. (2005, 2007) coupled the microphysical aerosol model MADE to the ECHAM4 general circulation model (GCM) and to the ECHAM5 GCM within the MESSy framework (Jöckel et al., 2006). Vignati and Wilson (2004) and Stier et al. (2005) developed the two-moment aerosol module HAM and implemented it into ECHAM5. The same microphysical core was included in the MESSy framework as the M7 submodel by Kerkweg et al. (2008). Ayash et al. (2008) implemented the sectional Canadian Aerosol Module (CAM) into the Third Generation Canadian Climate Center General Circulation Model (CCC GCM III).

The mixing state of the aerosol components has been represented in a very simplified manner by many global aerosol models. Some models treat aerosols as completely internally mixed (Adams et al., 1999), others as externally mixed (Chin et al., 2000), and some track separately hydrophobic, i.e. externally mixed, and hydrophilic, i.e. internally mixed, BC, while assuming a fixed turnover rate from the external into the internal mixture (e.g., Lauer et al., 2005; Lohmann et al., 1999; Koch, 2001). Only a few models explicitly resolve the mixing state of BC particles by simulating the relevant aging processes: for instance, Jacobson (2001b) developed a model that distinguishes between the two mixing states, and even among particles with different core-to-shell thickness ratio, but this model might be computationally too expensive to be used for long-term global climate simulations. Another example is KAMM/DRAIS-MADEsoot (Riemer et al., 2003), a mesoscale model that simulates mass and number concentrations of soluble aerosol and of internally and externally mixed BC particles. Along the same line, also process models have been developed. The aerosol model MADRID-BC (Oshima et al., 2009) can simulate changes in the BC mixing state resulting from condensation and evaporation processes. The stochastic particle-resolved model PartMC-MOSAIC (Riemer et al., 2009) explicitly resolves the composition of individual particles in a given population of different types of aerosol particles and, hence, tracks the evolution of the mixing state of particles due to emission, dilution, condensation, and coagulation. However, MADRID-BC and PartMC-MOSAIC have not been implemented into a regional or global model yet.

Among the global aerosol-climate models, not many can explicitly simulate the particles number concentration, size distribution, and mixing state. For instance, ECHAM5/HAM (Stier et al., 2005) distinguishes between internally and

externally mixed BC and dust, but does not predict the fraction of the total aerosol that does not contain any insoluble component. The global aerosol-climate models EMAC-M7 (Kerkweg et al., 2008) and EMAC-GMXe (Pringle et al., 2010) apply a similar aerosol description and microphysical core as ECHAM5/HAM. Another example is the GISS-ModelE/MATRIX (Bauer et al., 2008), which simulates an aerosol population composed of soluble particles, externally and internally mixed BC and externally and internally mixed dust. Similarly the CAM-Oslo (Seland et al., 2008) and NCAR-CAM3/IMPACT (Wang et al., 2009) global models can predict a variety of aerosol types in different states of mixing. In this work we present the new aerosol microphysics submodel MADE-in (modal aerosol dynamics model including insoluble modes). MADE-in is implemented within the ECHAM/MESSy global Atmospheric Chemistry model (EMAC, Jöckel et al., 2006). EMAC/MADE-in keeps track of soluble and insoluble sub-micrometer aerosol particles, simulating separately number, mass and size distributions of externally and internally mixed mineral dust and BC particles and of BC- and dust-free sub-micrometer aerosol. One of our goals is to couple EMAC/MADE-in with an ice microphysical scheme for investigating ice nuclei effects on cirrus clouds, including potential effects of BC from aviation. Therefore we focus on achieving a reliable description of aerosols in the upper troposphere and lowermost stratosphere (UTLS). The new model is described in Sect. 2. Section 3 shows the evaluation of the model with measurements. We compare the model with measured vertical profiles of aerosol concentrations and with surface measurements of aerosol mass, numbers and size distributions. A comparison with results from other global models is also presented in Sect. 3. Section 4 gives an example of a possible application of EMAC/MADE-in, and Sect. 5 presents the main conclusions of this study.

2 Model description

2.1 The aerosol microphysics model MADE-in

MADE-in is an aerosol dynamics model that allows for simulations of number concentration, size distribution and chemical composition of the atmospheric aerosol. Following the concept implemented by Riemer et al. (2003) in the frame of a regional model for the south-western part of Germany, MADE-in extends the original Modal Aerosol Dynamics Model for Europe (MADE) to the simulation of the number, size, and mixing state of black carbon and mineral dust particles. MADE has been developed as a part of the European Air Pollution Dispersion model system (EURAD) by Ackermann et al. (1998). Its core is based on the Regional Particulate Model (RPM) of Binkowski and Shankar (1995), who applied a modal representation of aerosol microphysical processes (Whitby et al., 1991) for studies of the North America

region. MADE was coupled to the general circulation model ECHAM4 by Lauer et al. (2005) and Lauer and Hendricks (2006), and later to ECHAM5 by Lauer et al. (2007) in the framework of the model system MESSy (Jöckel et al., 2005). The ECHAM5 version has been used here as the basis for the development of MADE-in.

The original aerosol microphysics model MADE describes the aerosol size distribution as a superposition of three log-normal modes: an Aitken mode, typically containing particles smaller than 100 nm, an accumulation mode, with a typical size range of 100 nm to 1 µm, and a coarse mode, for particles typically larger than 1 µm. All particles are assumed to be spherical and internally mixed. The Aitken and the accumulation modes are composed of SO_4, NH_4, NO_3, particulate organic matter (POM), water and BC. Additionally, the accumulation mode contains mineral dust and sea salt. The coarse mode is composed of water, mineral dust and sea salt. The model includes two separate representations for hydrophilic and hydrophobic BC and for hydrophilic and hydrophobic POM. MADE does not explicitly simulate the transformation of hydrophobic into hydrophilic particles, but includes a simplified representation of the aging process according to an exponential decay with an e-folding time of one day. Since mineral dust mostly has a very small soluble mass fraction, dust is assumed by MADE to be hydrophobic. Hence, mineral dust particles cannot be activated to form cloud droplets and are taken up by cloud and rain droplets via impact scavenging only. This, however, is a simplification as some measurements and theory show that some mineral dust particles can indeed act as cloud condensation nuclei and can form cloud droplets after gaining a coating of liquid solutions (e.g. Kelly et al., 2007; Andreae and Rosenfeld, 2008; Kumar et al., 2009; Sullivan et al., 2009). Since MADE focuses on the characterization of sub-micrometer aerosol, whose evolution is in a first order approximation not strongly influenced by coarse mode particles (Binkowski and Roselle, 2003), interactions of the coarse mode with the smaller modes are neglected.

MADE-in follows the same basic assumptions as MADE but with an extended number of modes to improve the representation of the aerosol mixing state. Furthermore, MADE-in simulates also the aging of mineral dust from hydrophobic to hydrophilic by gaining a soluble coating. Our major motivation for developing MADE-in is to provide more detailed aerosol simulations to be used for assessing aerosol-induced cirrus clouds formation in the UTLS (e.g. Hendricks et al., 2005). Therefore, we did not modify the representation of the coarse mode in MADE since, due to efficient gravitational settling, coarse mode particles are less abundant in the UTLS. Even during major dust storms, for instance, coarse mode particle number concentrations observed in the UTLS are very small (Weinzierl et al., 2009). The details of MADE-in are described below.
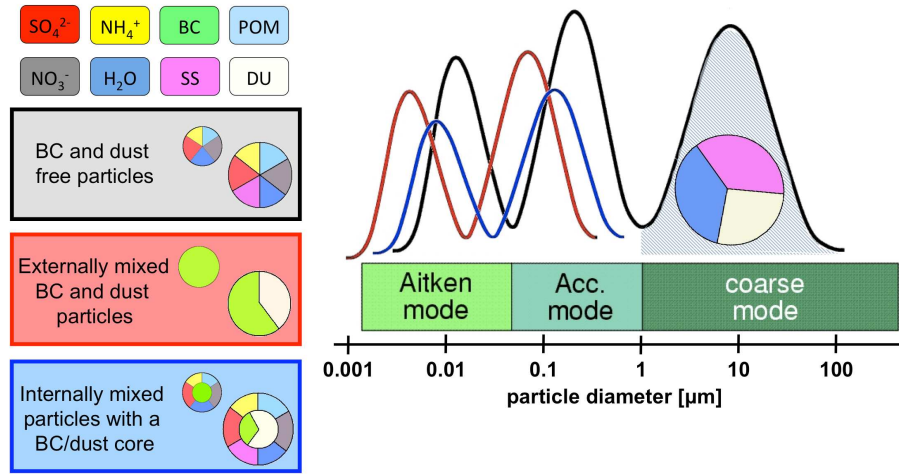
Fig. 1. Schematic representation of the aerosol distribution in MADE-in. BC indicates black carbon, POM particulate organic matter, SS sea salt and DU dust. The shaded mode is the coarse mode, which does not interact with the sub-micrometer modes. The black line depicts the fine modes without BC and dust, the red line the modes for externally mixed BC and dust particles and the blue line the modes for internally mixed BC and dust.

2.1.1 Representation of the aerosol population

MADE-in represents the aerosol number concentration by a superposition of seven log-normal modes. The particle number concentration $n(D)$ within each mode follows a lognormal distribution:

$$n(D) = \frac{dN}{dD} = \frac{N_t}{\sqrt{2\pi}\, D \ln \sigma_g} \exp\left[-\frac{(\ln D - \ln D_g)^2}{2 \ln^2 \sigma_g} \right], \quad (1)$$

where N_t is the total number concentration of the mode, D_g the median diameter and σ_g the geometric standard deviation. A detailed description of the modal approach can be found in Whitby and McMurry (1997). Each of the seven modes describes a different type of particles, characterized by particle size, composition and mixing state (Fig. 1). The seven MADE-in modes are:

– an Aitken mode (akn_{sol}) for internally mixed soluble particles. akn_{sol} particles are composed of SO$_4$, NH$_4$, NO$_3$, POM and water;

– an accumulation mode (acc_{sol}) for internally mixed soluble particles. acc_{sol} particles are composed of SO$_4$, NH$_4$, NO$_3$, POM, water and sea salt;

– an Aitken mode (akn_{ext}) for BC particles without or with only a thin soluble coating, following the definition given in Sect. 2.2. Particles with a thin coating probably show similar hygroscopic properties as externally mixed particles (Weingartner et al., 1997; Khalizov et al., 2009). Therefore we generally refer to these particles as externally mixed BC particles. The coating is composed of the same species as present in akn_{sol};

– an accumulation mode (acc_{ext}) for particles composed of BC and mineral dust without or with a thin soluble coating (externally mixed BC and dust). The coating is composed of the same species as present in acc_{sol};

– an Aitken mode (akn_{mix}) for BC particles with a thick coating. We refer to these particles as internally mixed BC particles;

– an accumulation mode (acc_{mix}) for BC and dust particles with a thick coating (internally mixed BC and dust particles);

– a coarse mode (cor) for particles typically larger than about 1 µm and composed of water, sea salt and dust.

Similarly to MADE, the Aitken modes typically contain particles smaller than 100 nm and the accumulation modes have a typical size range of 100 nm to 1 µm. The size range of one mode is not fixed, and can change due to microphysical processes. The growth of particles, for instance, shifts the diameter of the modes towards larger values. The nucleation of many small particles shifts the mode to smaller diameters. Aerosol mass and number can be transferred among the 6 sub-micrometer modes. If, for instance, Aitken mode particles grow into the size range of the accumulation mode, a part of the mass and number concentration of the Aitken mode is transferred to the accumulation mode. If externally mixed BC or dust particles acquire a soluble coating large enough to become internally mixed, they are transferred to the internally mixed modes with BC and dust. As MADE, MADE-in simulates the evolution of the coarse mode independently of the sub-micrometer modes, in order to reduce the computational demand. Within an individual mode, it is assumed that

Table 1. Chemical composition of the modes in MADE and in MADE-in. POM stands for particulate organic matter, BC for black carbon, DU for mineral dust and SS for sea salt. The externally mixed modes (akn_{ext}, acc_{ext}) contain some amount of soluble material. When this amount is large enough the externally mixed modes are transferred to the internally mixed ones (akn_{mix}, acc_{mix})

	SO_4	NH_4	NO_3	MADE POM	H_2O	SS	BC	DU
akn	×	×	×	×	×		×	
acc	×	×	×	×	×	×	×	×
cor					×	×		×

	SO_4	NH_4	NO_3	MADE-in POM	H_2O	SS	BC	DU
akn_{sol}	×	×	×	×	×			
acc_{sol}	×	×	×	×	×	×		
akn_{ext}	×	×	×	×	×		×	
acc_{ext}	×	×	×	×	×	×	×	×
akn_{mix}	×	×	×	×	×		×	
acc_{mix}	×	×	×	×	×	×	×	×
cor					×	×		×

all particles have the same composition. The seven modes of MADE-in are summarized and compared to those of MADE in Table 1. Internally and externally mixed BC or dust particles are assumed to be hydrophilic and hydrophobic, respectively. The standard deviation of each mode is fixed and set to 1.7, 2.0 and 2.2 for the Aitken, accumulation and coarse modes, respectively (Hess et al., 1998; Lauer et al., 2005).

MADE-in solves prognostic equations for the 0th and 3rd moments of each mode. The kth moment of a distribution is defined as

$$M^{(k)} = \int_{-\infty}^{+\infty} D^k n(\ln D) d(\ln D)$$
$$= N_t D_g{}^k \exp\left[\frac{k^2}{2}\ln^2\sigma_g\right], \quad (2)$$

where the last equivalence holds if $n(D)$ is a log-normal distribution. The 0th and 3rd moments are related to the total number N_t and total volume V_t of the mode through

$$M^{(0)} = N_t, \quad (3)$$

$$M^{(3)} = \frac{6}{\pi}V_t. \quad (4)$$

From Eqs. (2) and (3) the median diameter of the mode can be calculated as

$$D_g = \left[\frac{M^{(3)}}{M^{(0)}\exp\left[\frac{9}{2}\ln^2\sigma_g\right]}\right]^{1/3}. \quad (5)$$

Hence, the changes in the 0th and 3rd moments control the evolution of D_g.

2.1.2 Aerosol microphysics

The aerosol processes simulated by MADE-in are the following:

- condensation of sulfuric acid vapor and organic gases onto pre-existing aerosol;

- nucleation of sulfuric acid ($H_2SO_4(g)$) and water vapor forming new sulfate particles;

- coagulation of aerosol particles;

– gas/aerosol partitioning, i.e. the partitioning between nitric acid ($HNO_3(g)$) and ammonia ($NH_3(g)$) in the gas phase and nitrate (NO_3) and ammonium (NH_4) in the aerosol liquid phase, respectively, and the uptake of aerosol liquid water.

The individual representations of these processes are described below. MADE-in, as most aerosol models, uses the operator splitting approach, i.e. treats the microphysical processes consecutively within each time step. The order of the processes is chosen depending on their typical time scales. As in the base model MADE, gas/aerosol partitioning is calculated first, followed by condensation, nucleation and coagulation. These processes change the aerosol mass and number, possibly inducing changes in the median diameter of the modes (Eq. 5). This allows the Aitken mode particles to grow into the size range of the accumulation mode (Lauer et al., 2005). The aerosol model, then, assigns a fraction of the mass and number from the Aitken to the accumulation mode (mode merging, see below). Furthermore, gas/aerosol partitioning, condensation and coagulation can create or enlarge the coating on externally mixed BC and dust particles, eventually transferring them to an internal mixture. MADE-in simulates this aging of BC and dust particles by assigning the mass and number concentration of an externally mixed mode to the corresponding internally mixed modes with BC and dust, once the mass of the coating reaches a critical fraction (Sect. 2.2).

The prognostic equations for the number concentration of each mode, corresponding to the 0th moment, are

$$\frac{\partial N_i}{\partial t} = R(N_i) + \frac{\partial N_i}{\partial t}\bigg|_{\text{nucl}} + \frac{\partial N_i}{\partial t}\bigg|_{\text{coag}}$$
$$+ \frac{\partial N_i}{\partial t}\bigg|_{\text{growth}} + \frac{\partial N_i}{\partial t}\bigg|_{\text{aging}}, \tag{6}$$

$$\frac{\partial N_{\text{cor}}}{\partial t} = R(N_{\text{cor}}), \tag{7}$$

where the index i represents the individual sub-micrometer modes (akn_{sol}, acc_{sol}, akn_{ext}, acc_{ext}, akn_{mix} and acc_{mix}). $R(N_i)$ represents the change in the number concentration of the mode i due to transport (advection, convection, and diffusion), emissions, sedimentation and dry and wet deposition. These processes are not included in the aerosol submodel, but are handled by other submodels within the global model system EMAC (Sect. 2.3, Table 2). The other terms correspond to the change in the number concentration due to nucleation of H_2SO_4, coagulation, growth (transfer of Aitken mode particles into the accumulation mode) and aging, respectively. $\frac{\partial N_i}{\partial t}\big|_{\text{aging}}$ accounts for the number of particles that undergo aging due to condensation of sulfuric acid and/or organic vapor as well as uptake of water. The aging due to coagulation is included in $\frac{\partial N_i}{\partial t}\big|_{\text{coag}}$. Mode merging (growth) takes place

only between modes of the same family, i.e. only between akn_{sol} and acc_{sol}, between akn_{ext} and acc_{ext}, and between akn_{mix} and acc_{mix}.

The equations for the mass mixing ratios $C_{x,i}$ of the species x in the mode i are derived from the evolution of the 3rd moment of each mode, assuming that all particles within one mode have the same composition. The equations are

$$\frac{\partial C_{x,i}}{\partial t} = R(C_{x,i}) + \frac{\partial C_{x,i}}{\partial t}\bigg|_{\text{g/p}} + \frac{\partial C_{x,i}}{\partial t}\bigg|_{\text{cond}} \tag{8}$$
$$+ \frac{\partial C_{x,i}}{\partial t}\bigg|_{\text{nucl}} + \frac{\partial C_{x,i}}{\partial t}\bigg|_{\text{coag}}$$
$$+ \frac{\partial C_{x,i}}{\partial t}\bigg|_{\text{growth}} + \frac{\partial C_{x,i}}{\partial t}\bigg|_{\text{aging}},$$

$$\frac{\partial C_{x,\text{cor}}}{\partial t} = R(C_{x,\text{cor}}). \tag{9}$$

$R(C_{x,i})$ represents the change in the mass concentration of species x in mode i due to transport, emissions, sedimentation, dry deposition, wet deposition and chemistry. Besides the terms describing the change in the mass concentration due to nucleation, coagulation, growth and aging, Eq. (8) includes also the terms

$$\frac{\partial C_{x,i}}{\partial t}\bigg|_{\text{g/p}} \quad \text{and} \quad \frac{\partial C_{x,i}}{\partial t}\bigg|_{\text{cond}},$$

which describe the changes in NO_3, NH_4 and H_2O due to mass exchange between gas and particles and the increase in SO_4 and POM due to condensation of gases, respectively. These processes are not considered in Eq. (6) since they have no direct effect on the particle number concentration in the model. The details of representing the different processes in MADE-in are described in the following.

Gas/aerosol partitioning

The partitioning of nitric acid (HNO_3) and ammonia (NH_3) between gas and particle phase (NO_3 and NH_4) as well as the uptake of aerosol liquid water is calculated using the computationally efficient equilibrium model EQSAM (Metzger et al., 2002a,b). EQSAM assumes that the equilibrium activities of atmospheric aerosol species are controlled by relative humidity (RH), allowing for a parameterization of single solute molalities and activity coefficients only dependent on the type of solute and RH.

Since the equilibration time increases with particle size (Meng and Seinfeld, 1996), MADE-in applies EQSAM first to the Aitken modes and subsequently to the accumulation modes. The three modes within the respective modal size range (Aitken or accumulation mode) can show similar particle sizes, therefore the partitioning is calculated for the overall mass within each size range. That is, the mass concentrations of SO_4, NO_3, NH_4 and sea salt, respectively, in

Table 2. List of the EMAC submodels that have been used in this work.

Submodel	Function	Reference
CONVECT	Original ECHAM5 convection scheme	Tiedtke (1989); Nordeng (1994)
CVTRANS	Transport of tracers by convection	Tost et al. (2006b)
DRYDEP	Trace gas and aerosol dry deposition	Kerkweg et al. (2006a)
H2O	Initialization of H_2O in the stratosphere and mesosphere from satellite observations and feedback with specific humidity	Lelieveld et al. (2007)
JVAL	Calculation of photolysis rate coefficients	Landgraf and Crutzen (1998)
LNOX	Production of NO_X by lightning	Price and Rind (1992)
MADE-in	Aerosol microphysics	this study
MECCA	Tropospheric and stratospheric chemistry	Sander et al. (2005)
OFFLEM	Offline emissions	Kerkweg et al. (2006b)
ONLEM	Online emissions	Kerkweg et al. (2006b)
RAD4ALL	Original ECHAM5 radiation model	Roeckner et al. (2003)
SCAV	Wet deposition and liquid phase chemistry	Tost et al. (2006a, 2007)
SEDI	Sedimentation of aerosols	Kerkweg et al. (2006a)
TNUDGE	Nudging of tracers	Kerkweg et al. (2006b)
TROPOP	Calculation of the altitude of the tropopause	Jöckel et al. (2006)
CLOUD	Cloud physics	Lohmann (2002), Lohmann and Kärcher (2002)

the three Aitken modes are summed and the partitioning is then calculated for the total mass concentration of each compound. In the model set-up used in this work, sea salt is not included in the Aitken mode (Table 1), therefore the sea salt concentration is zero. The model, however, allows for the presence of sea salt in the Aitken mode, too. Aerosol liquid water, NO_3 and NH_4 calculated by EQSAM are then divided among the three Aitken modes according to their original relative contributions to the soluble material. The accumulation modes are treated in the same way. By this mechanism, a fraction of NO_3, NH_4 and water mass can be assigned also to the externally mixed modes, which can lead to the growth of their coating.

The partitioning between gas and aerosol does not change the aerosol number concentration, but alters the aerosol mass concentration of NO_3, NH_4 and water in the sub-micrometer modes. The terms of Eq. (8) corresponding to gas/aerosol partitioning are

$$\frac{\partial C_{NO_3,i}}{\partial t}\bigg|_{g/p}, \quad \frac{\partial C_{NH_4,i}}{\partial t}\bigg|_{g/p} \quad \text{and} \quad \frac{\partial C_{H_2O,i}}{\partial t}\bigg|_{g/p},$$

where i identifies the individual sub-micrometer modes.

Condensation of sulfuric acid and organic vapor

The condensation of sulfuric acid and organic vapor on pre-existing particles is calculated following Whitby et al. (1991). The mass of particulate SO_4 and POM gained from condensing vapor in each mode is proportional to the growth rates of the third moments $G_i^{(3)} = \partial M_i^{(3)}/\partial t$, which are cal-

culated as the harmonic mean of fluxes for the free-molecular and near-continuum regimes for each mode and each condensable species. The growth rates $G_i^{(3)}$ depend on the first and second moments of the aerosol modes, the vapor pressures and diffusion coefficients of sulfuric acid and organic gases, their sticking coefficients for soluble and insoluble particles, as well as other thermodynamic parameters such as the mean molecular velocity. More details on the calculation of the condensation coefficients are provided in Appendix A.

The terms of Eq. (8) corresponding to condensation of vapor are included in the model as

$$\frac{\partial C_{SO_4^{2-},i}}{\partial t}\bigg|_{cond} = \frac{G_{SO_4,i}^{(3)}}{\sum_{j=1}^{6} G_{SO_4,j}^{(3)}} \frac{\Delta C_{H_2SO_4}}{\Delta t}, \quad (10)$$

$$\frac{\partial C_{POM,i}}{\partial t}\bigg|_{cond} = \frac{G_{SOA,i}^{(3)}}{\sum_{j=1}^{6} G_{SOA,j}^{(3)}} \frac{\Delta C_{SOA}}{\Delta t}, \quad (11)$$

where i and j run over each of the six sub-micrometer modes and Δt is the time step. While the amount of condensing sulfuric acid vapor $\Delta C_{H_2SO_4}$ is calculated analytically from its production and loss rate, the condensable organic material ΔC_{SOA} is considered as an effective emission (Dentener et al., 2006).

Nucleation

The binary nucleation of water and sulfuric acid is parameterized following Vehkamäki et al. (2002). The nucleation rate

of new particles depends on temperature, relative humidity and the concentration of sulfuric acid vapor. The nucleation scheme is called by the model after condensation has been considered. Hence, only the amount of sulfuric acid vapor not consumed by condensation is available for nucleation of new particles. The used parameterization is applicable for temperatures in the range of 190.15–300.15 K, for relative humidities of 0.01 %–100 %, and sulfuric acid vapor concentrations of 10^4–10^{11} molecules cm^{-3}. The resulting nucleation rate is in the range of 10^{-7}–10^{10} particles/(cm^3 s). The mass production corresponding to the nucleation rate is calculated assuming that the freshly nucleated particles are lognormally distributed with a wet median diameter of 3.5 nm and the standard deviation of the Aitken mode. Nucleation can result in a large contribution to the total number of particles in the Aitken mode. The simulated effects on particle mass concentration, however, are mostly small (Lauer and Hendricks, 2006). The freshly nucleated sulfate particles are assigned to the Aitken mode without BC and dust. The corresponding terms in Eqs. (6) and (8) are

$$\frac{\partial N_{akn}}{\partial t}\bigg|_{nucl} = J(T, RH, C_{H_2SO_4}), \qquad (12)$$

$$\frac{\partial C_{SO_4^{2-}, akn}}{\partial t}\bigg|_{nucl} = J(T, RH, C_{H_2SO_4}) \times \qquad (13)$$

$$m_{3.5}(RH)\exp\left[\frac{9}{2}\ln^2\sigma_{akn}\right],$$

where J is the nucleation rate and $m_{3.5}$ denotes the mass of sulfate contained in a spherical particle with a wet diameter of 3.5 nm, calculated as a function of the relative humidity fitting experimental data (Vehkamäki et al., 2002).

Coagulation

Coagulation is the process of collision and sticking of aerosol particles and the resulting formation of larger particles. The coagulation rates in the model are calculated for spherical particles as a function of the median diameter of the coagulating modes following Binkowski and Shankar (1995). The rates are higher for interactions between particles with different diameters than for particles of the same size. Only coagulation due to Brownian motion is considered and it is assumed that the aerosol distribution remains log-normal after the coagulation process. MADE-in simulates the coagulation between particles of the same mode (intramodal coagulation) and of different modes (intermodal coagulation).

The following assumptions are made:

- particles resulting from intramodal coagulation remain in the same mode as the coagulating particles;

- particles resulting from intermodal coagulation are assigned to the larger of the coagulating modes;

- particles resulting from coagulation of a BC and dust free mode (akn$_{sol}$ or acc$_{sol}$) and an internally mixed mode with BC or dust (akn$_{mix}$ or acc$_{mix}$) are assigned to akn$_{mix}$ or acc$_{mix}$;

- particles resulting from coagulation of an externally mixed BC and dust mode (akn$_{ext}$ or acc$_{ext}$) and an internally mixed mode (akn$_{mix}$, acc$_{mix}$, akn$_{sol}$ or acc$_{sol}$) are assigned to akn$_{mix}$ or acc$_{mix}$ if the soluble mass fraction of the new particle exceeds a given threshold (Sect. 2.2). Otherwise, the new particle is assigned to the coagulating externally mixed mode.

Table 3 shows all possible coagulation pathways considered in the model as well as the modes the new particles are assigned to. While intramodal coagulation conserves the mass of the mode, intermodal coagulation can change both the modes' number and mass concentrations. If, for instance, a large enough soluble particle from acc$_{sol}$ coagulates with an externally mixed BC particle from akn$_{ext}$, the resulting aerosol will be an internally mixed BC particle in the acc$_{mix}$ mode. The mass and number concentration of acc$_{sol}$ and akn$_{ext}$ will decrease, while the mass and number concentrations of acc$_{mix}$ increase. The coagulation terms in Eqs. (6) and (8) are

$$\frac{\partial N_i}{\partial t}\bigg|_{coag} = \frac{\partial N_i}{\partial t}\bigg|_{inter-coag} + \frac{\partial N_i}{\partial t}\bigg|_{intra-coag}, \qquad (14)$$

$$\frac{\partial C_{x,i}}{\partial t}\bigg|_{coag} = \frac{\partial C_{x,i}}{\partial t}\bigg|_{inter-coag} \qquad (15)$$

$$= \frac{1}{M_i^{(3)}}\frac{\partial M_i^{(3)}}{\partial t}\bigg|_{inter-coag} C_{x,i}.$$

More details about the calculation of the coagulation coefficients are given in Appendix B.

Particle growth

The microphysical processes simulated by MADE-in can induce changes in the median diameter of the modes, so that the Aitken mode and the accumulation mode may overlap and become indistinguishable over time. To avoid this, a fraction of the Aitken mode is transferred to the accumulation mode in case of increasing overlap. The new median diameters are then calculated from Eq. (5). This algorithm is called mode merging. MADE-in performs mode merging between akn$_{sol}$ and acc$_{sol}$, between akn$_{ext}$ and acc$_{ext}$ and between akn$_{mix}$ and acc$_{mix}$. If the growth rate of the 3rd moment of an Aitken mode becomes larger than the one of the corresponding accumulation mode, MADE-in transfers the number of Aitken mode particles larger than D_N to the accumulation mode, where D_N is the intersection diameter between the number distributions of the two modes. The intersection diameter is calculated from the number size distributions (Eq. 1), imposing that the number concentrations

Table 3. Destination mode of each possible coagulation event in MADE-in. The first row and the first column show the coagulating modes.

	akn_{sol}	acc_{sol}	akn_{ext}	acc_{ext}	akn_{mix}	acc_{mix}
akn_{sol}	akn_{sol}	acc_{sol}	akn_{mix} or akn_{ext}	acc_{mix} or acc_{ext}	akn_{mix}	acc_{mix}
acc_{sol}		acc_{sol}	acc_{mix} or akn_{ext}	acc_{mix} or acc_{ext}	acc_{mix}	acc_{mix}
akn_{ext}			akn_{ext}	acc_{ext}	akn_{mix} or akn_{ext}	acc_{mix} or akn_{ext}
acc_{ext}				acc_{ext}	acc_{mix} or acc_{ext}	acc_{mix} or acc_{ext}
akn_{mix}					akn_{mix}	acc_{mix}
acc_{mix}						acc_{mix}

of the Aitken and of the accumulation modes at D_{N} are the same. The number of particles with diameter smaller than D_{N} is given by

$$N(D_{\text{N}}) = \frac{N_{\text{t}}}{2} + \frac{N_{\text{t}}}{2}\,\text{erf}\left(\frac{\ln(D_{\text{N}}/D_{\text{g}})}{\sqrt{2}\ln\sigma_{\text{g}}}\right), \qquad (16)$$

where the error function $\text{erf}(z)$ is defined as

$$\text{erf}(z) = \frac{2}{\sqrt{\pi}}\int_0^z e^{-\eta^2}\,d\eta, \qquad (17)$$

with $\text{erf}(0) = 0$ and $\text{erf}(\infty) = 1$. These particles are assumed to remain in the mode. In a similar manner, a fraction of the mass of the Aitken mode is transferred to the accumulation mode. More details about the technical aspects of the algorithm used can be found in Binkowski and Roselle (2003).

2.2 Aging of black carbon and dust particles

Coagulation and condensation of gases on externally mixed BC and mineral dust can create a coating around these particles and, therefore, transfer them to an internal mixture. Photochemical reactions can also contribute to the aging of externally mixed BC particles, transforming the surface from hydrophobic to hydrophilic. While Weingartner et al. (1997)

showed that aging via photochemical reactions is usually less efficient than via coagulation or condensation, Kotzick and Niessner (1999) stated that oxidation by ozone could be more important than coagulation in the change of the hygroscopic behavior. However, they used a high ozone concentration compared to typical tropospheric values.

In most global aerosol models the transformation of BC and dust from external to internal mixture is simulated in a very simplified way, assuming a fixed turnover rate. Lauer et al. (2005), Lohmann et al. (1999) and Koch (2001), for instance, assumed that the externally mixed BC is transformed into an internal mixture following

$$C_{\text{ext BC}}(t) = C_{\text{ext BC}}(t_0)e^{-\frac{1}{\tau}\cdot(t-t_0)}. \qquad (18)$$

The e-folding time τ was assumed to be 24 h by Lauer et al. (2005), 40 h by Lohmann et al. (1999) and 43 h by Koch (2001). In contrast, the 6 sub-micrometer modes of MADE-in allow to keep track of externally and internally mixed BC and dust throughout the calculation of aerosol microphysics. MADE-in can explicitly simulate aging of BC and dust by condensation of SO_4 and organic material, coagulation as well as uptake of nitrate, ammonium and water. If the amount of liquid mass (SO_4, NH_4, NO_3, POM, H_2O, sea salt) in an externally mixed mode i is larger than a critical relative fraction x of the total mass of the mode, the whole mass

and number of mode i are transferred to the internally mixed Aitken and accumulation modes with black carbon and dust (akn_{mix} and acc_{mix}). The intersection diameter between akn_{mix} and acc_{mix} is calculated and the externally mixed particles smaller than this diameter are assigned to akn_{mix}, the others to acc_{mix}. The mass fraction x is a free parameter of the model. Weingartner et al. (1997) and Khalizov et al. (2009) presented experimental studies on the properties of externally and internally mixed BC, suggesting that particles with a soluble mass fraction larger than 10% show a hygroscopic behavior. Following these results, in this study x is set to 10%.

Aging of black carbon and dust particles can also occur due to cloud processing (Matsuki et al., 2010). Externally mixed black carbon and dust particles incorporated in cloud droplets can remain as immersions within liquid cloud residual aerosol after cloud evaporation. Therefore, the scavenging submodel SCAV (Sect. 2.3) has been modified to simulate this process. Externally mixed BC and dust particles that are scavenged by cloud droplets but not removed by precipitation are assumed to be aged after the evaporation of the cloud, and are transferred to the internally mixed modes. A cloud droplet formed by an activated soluble accumulation mode particle can scavenge an Aitken mode particle containing BC. If the cloud droplet evaporates, the two aerosol particles remain as a merged cloud residue. Therefore, the mass of the two particles in the cloud droplet is transferred to the internally mixed accumulation mode containing insoluble mass. The number concentration $N_{transferred}$ of soluble particles that is contaminated by Aitken mode BC is calculated from the number concentrations of the particles that are taken up by cloud droplets as

$$N_{transferred} =$$
$$\min\left[\frac{N_{acc_{sol}}\big|^{cl}}{N_{acc_{tot}}\big|^{cl}} (N_{akn_{mix}}\big|^{cl} + N_{akn_{ext}}\big|^{cl}), N_{acc_{sol}}\big|^{cl}\right], \quad (19)$$

where the number concentrations labelled with index "cl" refer to aerosol taken up by cloud particles. It is assumed here that only accumulation mode particles can be activated. $N_{acc_{tot}}\big|^{cl}$ is the total number of accumulation mode particles in cloud droplets. $N_{transferred}$ denotes the number of particles that is transferred from the soluble accumulation mode to the internally mixed modes containing BC. The Aitken mode BC particles merged with acc_{mix} and acc_{ext} within cloud particles do not induce transfer of particles between soluble and insoluble modes, because these accumulation modes already contain insoluble mass. However, they induce a transfer of mass from the Aitken modes containing BC to the internally mixed accumulation mode containing BC. If more accumulation mode particles are scavenged than Aitken mode BC particles, it is assumed that each accumulation mode particle merges with at most one

Aitken mode BC particle. If more Aitken mode BC particles are scavenged than accumulation mode particles, all scavenged soluble accumulation mode particles are transferred to the internally mixed accumulation mode with BC and $N_{transferred} = N_{acc_{sol}}\big|^{cl}$. Note that the Aitken mode does not contain mineral dust, owing to the comparatively large sizes of mineral dust particles.

2.3 The ECHAM/MESSy Atmospheric Chemistry model

The ECHAM/MESSy Atmospheric Chemistry model (EMAC) is a numerical chemistry-climate simulation system that includes submodels describing tropospheric and middle atmosphere processes (Jöckel et al., 2005, 2006). It uses the first version of the Modular Earth Submodel System (MESSy1) to link multi-institutional computer codes. The core is the general circulation model ECHAM5 (Roeckner et al., 2006). ECHAM5 is a spectral model based on the primitive equations for momentum, temperature and moisture. The prognostic variables are vorticity, divergence, temperature, specific humidity and logarithm of the surface pressure. Except for the specific humidity, which is calculated in the grid point space, the prognostic variables are represented in the spectral space by a truncated series of spherical harmonics. The chosen truncation determines the horizontal resolution of the model.

For the present study we apply EMAC (ECHAM5 version 5.3.01, MESSy version 1.4) in the T42L19-resolution, i.e. with a spherical truncation of T42, corresponding to a quadratic Gaussian grid of approximately 2.8 by 2.8 degrees in latitude and longitude, and 19 vertical hybrid pressure levels. The atmosphere up to 10 hPa is divided in non-equidistant levels with a hybrid representation that follows the orography close to the surface and flattens in the UTLS. The standard ECHAM5 time step for the resolution T42L19 is 30 min, but it has been set here to 24 min to reach a higher model stability. The model results shown in this work are climatological averages over 10 yr of not nudged simulations (free running climate mode) after a spin-up period of one year. The assumed sea surface temperatures and ice cover fractions are based on the climatological mean of the Hadley Center data set (Rayner et al., 2003) over the period 1995–2004.

The applied model set-up comprises the submodels listed in Table 2. The gas- and liquid-phase chemistry is calculated by the submodels MECCA (Sander et al., 2005, Module Efficiently Calculating the Chemistry of the Atmosphere) and SCAV (Tost et al., 2006a, 2007), respectively. The model set-up used in this work includes a basic tropospheric background gas-phase (NO_x, HO_x, CH_4, CO, O_3) and sulfur chemistry (DMS, SO_2). The complete list of chemical mechanism considered in this work is included

in the supporting material. The amount of H_2SO_4, nitric acid and ammonia used by MADE-in for condensation and gas/aerosol partitioning is provided online by EMAC.

The emissions of aerosol and aerosol precursors are simulated by the submodels ONLEM and OFFLEM (Kerkweg et al., 2006b), which are responsible for online and prescribed (offline) emissions, respectively. We use prescribed emissions for all species except for sea salt and dimethyl sulfide (DMS), which are handled as described below. The emissions of trace gases other than SO_2 and DMS are chosen according to the EDGARv3.2-FT2000 inventory. The corresponding emission totals are reported by Pozzer et al. (2007). We use the emissions of aerosols and SO_2 for the year 2000 as recommended by Dentener et al. (2006) for the AeroCom project. 80% of the emitted BC is assumed to be hydrophobic and is, therefore, assigned to the externally mixed modes akn_{ext} and acc_{ext}. The remaining 20% is assigned to the internally mixed modes akn_{mix} and acc_{mix}. We assume the size distributions suggested by Dentener et al. (2006) for the emissions of primary particles. The number of particles emitted in the Aitken mode is calculated assuming a number size distribution with median radius 0.015 μm and standard deviation 1.8. For deriving the number of particles emitted in the accumulation mode a median radius of 0.04 μm and a standard deviation of 1.8 are assumed, except for mineral dust and sea salt. The dust particle number emissions fluxes are considered as calculated by Dentener et al. (2006) taking into account variable size distributions. The emitted dust is assigned to the coarse mode (1664 Tg per year) and to the externally mixed accumulation mode acc_{ext} (10.6 Tg per year), since the major emission regions of dust are usually poor in soluble material.

In the present model set-up sea salt and marine DMS are emitted online, i.e. the emissions are calculated from simulated model variables (Kerkweg et al., 2006b). Following Guelle et al. (2001), the mass and number fluxes of sea salt are calculated as a function of wind speed at 10 m using the empirical formulas by Monahan et al. (1986) for particles smaller than 4 μm and by Smith and Harrison (1998) for particles larger than 4 μm. Sea salt particles are assigned to the soluble accumulation and coarse mode (acc_{sol} and cor). Marine DMS emissions are calculated online using the empirical formula by Liss and Merlivat (1986) as a function of DMS concentrations in water and wind speed at 10 m.

For our simulations we use the two moment cloud microphysics scheme by Lohmann (2002), with extensions by Lohmann and Kärcher (2002), which is not part of the standard EMAC. The cloud scheme considers the cloud liquid water content, cloud ice water content, and the number concentrations of cloud droplets and ice crystals as prognostic variables. The number of aerosols activated to form cloud droplets is calculated by MADE-in following Abdul-Razzak and Ghan (2000) and is used as input for the cloud microphysics scheme. Only hydrophilic particles can be activated to form cloud droplets.

The scavenging of aerosol particles is parameterized by the submodel SCAV (Tost et al., 2006a, 2007). SCAV simulates nucleation and impaction scavenging of aerosol particles both in convective and large-scale clouds. We consider externally mixed BC and dust particles as hydrophobic, and, therefore, they are not scavenged via nucleation scavenging. We extended the standard version of SCAV included in MESSy 1.4 for a more detailed description of UTLS processes. In the original version of SCAV the aerosol that has been taken up by cloud particles (liquid water droplets or ice particles) is washed out according to the rain formation rate. Snow formation is neglected. This simplification is accurate enough in the lower troposphere, where snow is less frequent than rain. In the UTLS, however, the consideration of snow formation is crucial. Hence, this approach leads to an underestimation of aerosol wet removal. We modified SCAV in order to consider also aerosol removal in clouds due to snow formation. Following Lauer et al. (2005), we assume that 5% of the soluble aerosol mass is scavenged by ice crystals. In order to account for the ability of insoluble particles to act as ice nuclei, we use higher ice scavenging coefficients, equal to 10%, for particles containing BC or dust, either internally or externally mixed.

The dry deposition of trace gases and aerosols is calculated by the submodel DRYDEP (Kerkweg et al., 2006a). With dry deposition we denote the collision of aerosols with the surface due to turbulent motion and the subsequent sticking. DRYDEP calculates the dry deposition flux using the big leaf approach, depending on the near-surface turbulence and on the properties of the surface (Ganzeveld and Lelieveld, 1995). Dry deposition is only applied to the lowermost model layer.

The sedimentation of aerosol due to gravitational settling is calculated by the SEDI submodel (Kerkweg et al., 2006a) in all model layers. A simple upwind scheme and a trapezoid scheme are available in SEDI to calculate the change in particle concentration due to sedimentation. In this work we use the simple upwind scheme: the fraction of particles falling from one box into the next box below is calculated from the geometric vertical extension of the box and the terminal velocity of the aerosol particles for each time step. It is assumed that the particles of one grid box are homogeneously distributed with height.

The aerosol optical properties are calculated by MADE-in following Lauer et al. (2007), depending on the chemical composition and particle size. The refractive index of each mode is calculated under the assumption of internal mixture as the average of the refractive index of the individual species, weighted with their relative volume contribution (Ouimette and Flagan, 1982). The refractive index and the wet radius of the mode are used to identify the extinction cross section, single scattering albedo, and asymmetry factor of the particles in previously generated look-up tables. The look-up tables have been calculated by Lauer et al. (2007) from Mie theory using the libRadtran code (Mayer

and Kylling, 2005). The aerosol optical properties calculated by MADE-in are then used by EMAC in the calculation of the short and long-wave radiation fluxes.

3 Comparison with observations

In the present study, EMAC/MADE-in was applied as described in Sect. 2.3. The aerosol population simulated with this model set-up for the lower troposphere is very similar to the one calculated by EMAC/MADE, which has been extensively evaluated with observations (Lauer et al., 2005, 2007). However, the new representation of aerosol and different parameterizations of aerosol sinks introduced in EMAC/MADE-in makes a reevaluation of the model system necessary. While EMAC/MADE is mainly designed to model lower tropospheric aerosol, EMAC/MADE-in aims at describing aerosols also at higher altitudes. Comparisons of EMAC/MADE-in results with observational data are discussed in the following.

3.1 Aerosol mass concentration

The vertical profiles of the simulated aerosol mass concentrations are compared with measurements taken with an airborne Single Particle Soot Photometer (SP2) over Texas by Schwarz et al. (2006) in November 2004, over Costa Rica during the CR-AVE (Schwarz et al., 2008) and TC4 campaigns (Spackman et al., 2010) in February 2006 and August 2007, respectively, and over northern Europe during the CIRRUS campaign (Baumgardner et al., 2008) in November 2006. Figure 2 shows the comparison of simulated and measured mass concentrations of BC, total aerosol and particles with no detectable BC. Mean and standard deviation are not always well suited to capture the variability of the data, because the distributions of aerosol mass can be non-Gaussian or strongly asymmetric. Hence, medians and percentiles are also plotted when available. For clarity, only positive standard deviations are drawn for the simulated concentrations as well as for the CIRRUS data.

The simulated mass mixing ratios shown in Fig. 2 represent climatological 10-yr means simulated by EMAC/MADE-in for the month the respective campaign took place. In the case of the Texas campaign and of CIRRUS, the exact profiles of the flights are available. Therefore, we considered the aerosol mixing ratios of the model grid boxes containing the flight routes. In the case of TC4 and CR-AVE only the boundaries of the examined region are considered. The simulated profiles have been averaged over a rectangular region containing the flight routes (80° W–92° W, 2° N–12° N for TC4 and 79° W–85° W, 1° S–11° N for CR-AVE). The experimental data are averaged over 1-km vertical bins. The observations during the CIRRUS, CR-AVE and TC4 campaigns were obtained in cloud-free air; therefore the averages of the simulated

mixing ratios have been calculated including only those cases where the cloud cover is lower than 1%. The results are not very sensitive to this threshold: choosing a higher threshold such as, for instance, 5% or 10% results in a slight increase in the simulated aerosol mass. Figure 2 shows also the aerosol mass mixing ratio simulated by EMAC/MADE (Lauer et al., 2007). Up to 900 hPa (700 hPa in the case of Texas) the mixing ratios simulated by EMAC/MADE and by EMAC/MADE-in are similar. They diverge above this layer, where EMAC/MADE simulates aerosol mixing ratios much higher than both the measurements and EMAC/MADE-in. The improvement in the simulation of the vertical profiles is mainly due to the different representation of ice scavenging (Sect. 2.3), which is underestimated in EMAC/MADE. The profiles simulated with EMAC/MADE-in agree reasonably well with the observations, especially in the UTLS. The simulated total aerosol mixing ratio over Texas (Fig. 2b) is larger than the observed one, but it reproduces the observed vertical gradient quite well.

The CIRRUS campaign took place over Europe between 50° N and 70° N. The anthropogenic aerosol sources are mainly concentrated in the southern part of this region, causing often a strong latitudinal gradient in the aerosol concentrations. While the simulated BC vertical profile shows lower concentrations than the measured one, the profile of the mass concentration of BC-free aerosol is in very good agreement with the experimental data. This discrepancy may be related to the fact that the sources of BC free particles are more homogeneously distributed over the observed area than the BC sources; therefore, their concentration is less sensitive to meteorological conditions and specific transport patterns of the air masses during the campaign, which may differ from the mean transport pattern of the model. Furthermore, BC free aerosol is to a large fraction composed of secondary aerosol species. The concentration of secondary aerosol species is more homogeneous, because wet deposition is less effective on the precursor gases than on BC and hence they can be transported over long distances before they are transformed to aerosol.

The mass concentration of BC simulated by EMAC/MADE-in is compared with surface measurements from various sites in Fig. 3. For each observational data point we calculate the climatological means of all months covered by the observational time periods in the model grid boxes containing the measurement sites. The observations are taken from Chung and Seinfeld (2002), Cooke et al. (1999), Köhler et al. (2001), Liousse et al. (1996) and Takemura et al. (2000). Additionally, measurements by the Interagency Monitoring of Protected Visual Environments (IMPROVE, DeBell et al., 2006) network are used for North America.

The ratio between simulated and observed BC concentration is mostly between 0.1 and 10. Table 4 presents the mean ratio between the simulated and the observed concentrations. The comparison shows that the model underestimates BC
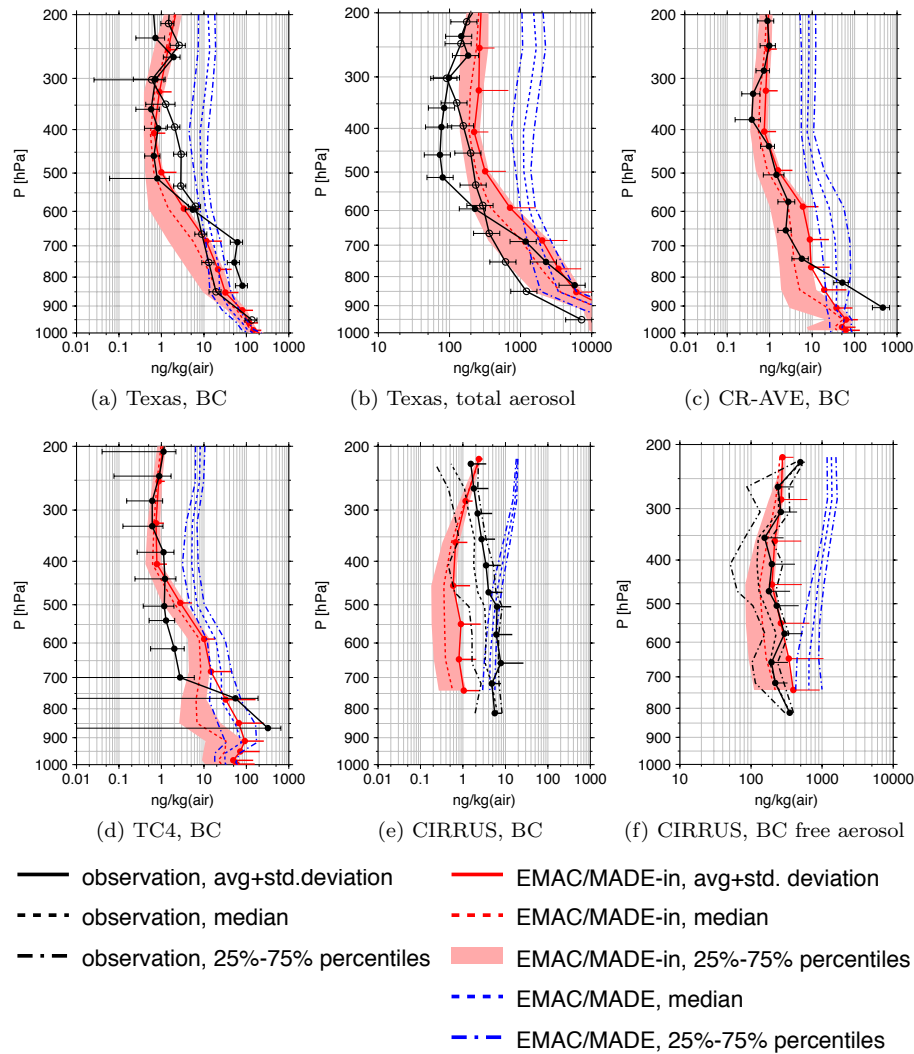
Fig. 2. Vertical profiles of BC and total aerosol mass (**a** and **b**, respectively) measured over Texas (Schwarz et al., 2006), of BC over Costa Rica during the CR-AVE campaign (**c**, Schwarz et al., 2008) and during the TC4 campaign (**d**, Spackman et al., 2010), and of BC and BC free particles over Europe during CIRRUS (**e** and **f**, respectively, Baumgardner et al., 2008) and corresponding model values of EMAC/MADE-in and EMAC/MADE. Open and solid circles in (**a**) and (**b**) correspond to two different flights. For clarity, only positive standard deviations are shown when median and percentile values are available.

mass concentration in the Pacific area. While the emissions of BC in the other five regions are mainly due to fossil fuel combustion, as in North America, Southeast Asia and Europe, or biomass burning, as in Africa and South America, the only emissions source of BC in the Pacific Ocean is shipping. Since the signal from shipping is expected to be small (Eyring et al., 2005), the simulated concentrations of BC represent background BC resulting from long-range transport. Hence, either the transport patterns or the residence time of BC over the Pacific could be misrepresented by the model. On the other hand, since the measurements sites are often located on islands they could be close to BC sources that are of sub-grid scale in the model. In such cases, the large

scale grid box mean values can be expected to be significantly smaller than the observed concentrations.

The simulated mass concentrations of BC, organic carbon (OC), SO_4 and NO_3 have been compared with surface measurements from the IMPROVE network, an extensive long-term program started in 1985 to monitor the visibility and aerosol conditions in the National Parks and Wilderness Areas in the USA (Fig. 4). Each participating station measures the total $PM_{2.5}$ and PM_{10} mass concentrations and, for $PM_{2.5}$, the mass concentrations of sulfate, nitrate, chloride, BC and OC twice a week for 24 h. The total SO_4, NO_3, BC and POM mass concentrations simulated by EMAC/MADE-in in the lowest level are compared to the corresponding
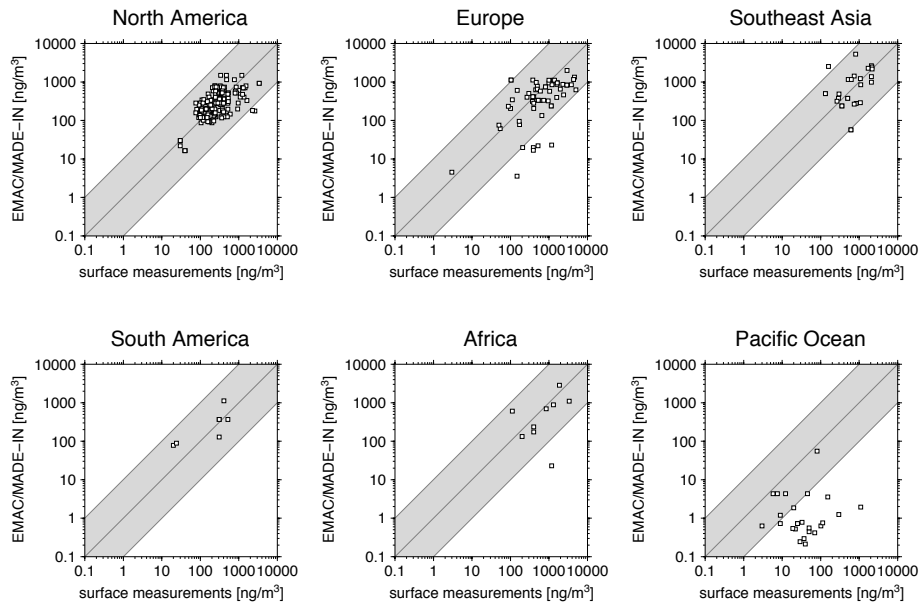
Fig. 3. Comparison of modeled and observed BC mass concentrations at surface level for different regions. Each square corresponds to one measurement site. The shaded regions indicate a ratio of measurements to model results within the range of 0.1 and 10. See text for more details on the observational data used.

Table 4. Mean ratio between the simulated and observed BC mass concentrations (model/obs.) shown in Fig. 3 and number of data points in each panel of Fig. 3 (pairs).

	Pairs	Model/obs.
North America	200	1.23
Europe	65	1.14
Southeast Asia	29	1.79
South America	6	1.97
Africa	9	1.16
Pacific Ocean	25	0.13

Table 5. Mean ratio between the simulated and observed aerosol mass concentrations of the data presented in Fig. 4 and number of stations considered for the comparison (pairs).

|	Pairs	Model/obs.
BC	96	0.99
OC	96	1.07
SO_4	96	2.01
NO_3	96	0.91

than those derived from the satellite observations. Table 5 shows the mean ratio between the simulated and observed mass concentrations for each compared species. In general, the model overestimates SO_4. This could be related to the fact that the IMPROVE measurement stations are in natural parks, where air is particularly clean. Since important sources of SO_4 are anthropogenic (Dentener et al., 2006), the interpolation over the whole USA obtained from the IM-PROVE data set is probably biased towards low concentrations. Additionally, as pointed out by Stier et al. (2005), the dry deposition scheme applied by DRYDEP (Ganzeveld et al., 1998) tends to underestimate the dry deposition velocity for SO_2, and, therefore, to overestimate the concentration of sulfate precursors. The model tends to underestimate nitrate. A possible reason could be that the simplified gas phase chemical scheme applied here results in lower HNO_3 concentrations as suggested by more comprehensive chemistry simulations as, for instance, by Jöckel et al. (2006).

IMPROVE PM$_{2.5}$ data taken between 1995 and 2005. The simulated mass concentration of POM has been divided by the factor 1.4 (Dentener et al., 2006) to compare it with observed OC.

The patterns of the mass concentrations of each species are well reproduced by the model, particularly those of BC and OC (Fig. 4, first and second panels). The maximum between north Idaho and west Montana, present in both the observations and the model results, is probably caused by very strong forest fires that took place in year 2000 in that region. These forest fires are included in the satellite based GFED database that we employed. The values reproduced by the model are lower than those observed. This may be due to the location of the IMPROVE stations: if they were particularly close to the fires, the values from surface measurements may be larger

Fig. 4. Comparison of the climatological annual mean of BC, OC, SO$_4$ and NO$_3$ in PM$_{2.5}$ from observations by the IMPROVE network (left column) and EMAC/MADE-in (right column). The crosses indicate the locations of the measurement sites. See text for more details.

Figure 5 shows a comparison between modeled and observed dust mass concentrations at the Earth's surface. The observed mean concentrations are taken from Huneeus et al. (2010), who presented a comparison of simulations by different models participating in the AeroCom project and observational data. The observations were performed at different stations all over the globe (Prospero et al., 1989; Arimoto et al., 1995; Prospero, 1996; Maenhaut et al., 2000a,b; Vanderzalm et al., 2003; Nyanganyura et al., 2007). The position

of the measurement stations is shown in Fig. 6. Stations 1 to 7, 8 to 16, and 17 to 22 are characterized by low, medium, and high dust surface concentrations, respectively. The simulated surface dust concentrations are smaller than the observed values at nearly all of the considered locations. Particularly, the large concentrations downwind the Saharan an Asian dust sources (stations 17 to 22) cannot be reproduced. This can be due to the consideration of a dust emission climatology in the model (Sect. 2.3), based on monthly mean dust

(a) Observations (b) Model results
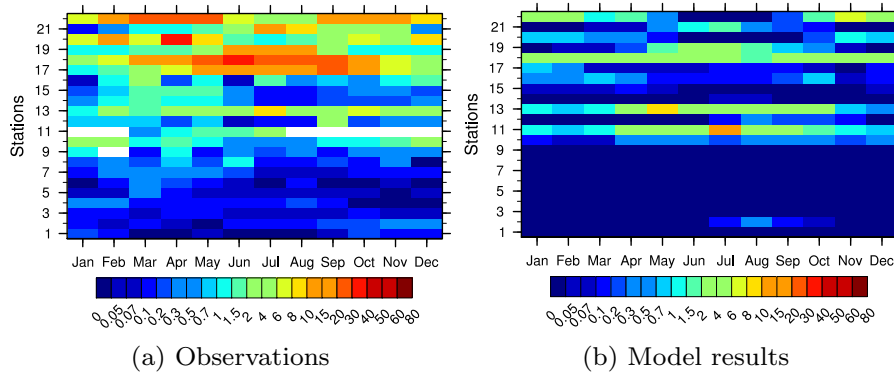
Fig. 5. Monthly averages of measured and simulated dust surface concentrations in µg m^{-3}. Observations are considered according to Huneeus et al. (2010). The location of the measurement stations is shown in Fig. 6.

emission fluxes. In cases of high wind speeds during specific episodes when the dust emissions should be particularly high and long-range dispersion is most efficient, the mean dust emission fluxes in the model may be too low and, consequently, the concentrations in the major dust plumes are underestimated. Another possible reason is that too little emitted dust mass is assigned to the accumulation mode. Sensitivity studies we performed with EMAC/MADE with different assumptions on the splitting of the emitted dust mass into coarse and accumulation mode mass demonstrate that the atmospheric dust burden in the model is very sensitive to these assumptions (not shown). Due to a less efficient gravitational settling, accumulation mode dust particles have larger residence times than coarse mode particles. Hence, shifting the splitting of the emitted dust mass towards the accumulation mode increases the atmospheric dust burden. Another possibility is that the efficiency of large particle removal is overestimated in the model, for instance, due to uncertainties in the representation of gravitational settling. Further studies are required to resolve these issues and to refine the representation of the dust load in the model.
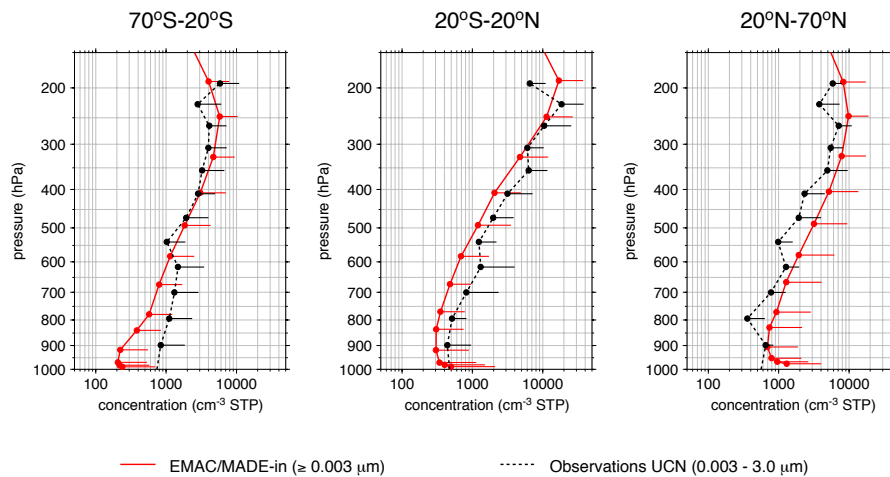
3.2 Aerosol number concentration

Vertical profiles of the aerosol number concentrations are compared with observations taken during several campaigns. When available, median values and percentiles are used instead of means and standard deviations to better account for the variability of aerosol number concentrations (Sect. 3.1). Figure 7 shows the comparison of aerosol number concentrations simulated by EMAC/MADE-in with observations from Clarke and Kapustin (2002) between 70° S and 70° N over the Pacific ocean. The observed profiles average data taken during the GLOBE-2 (May 1990), ACE-1 (November 1995) and PEM-Tropics A (September 1996) and B (March 1999) campaigns, using an ultrafine condensation nuclei (UCN) counter to detect particles with diameters between 3 nm and
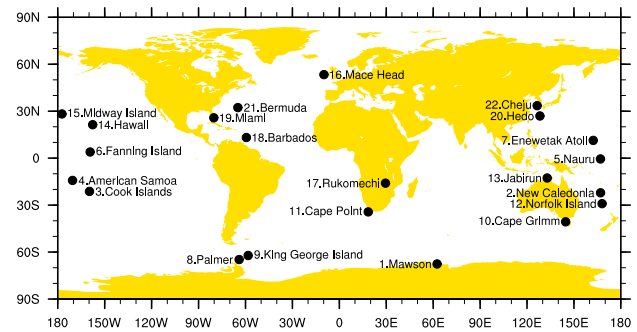

Fig. 6. Locations of the measurement stations analyzed by Huneeus et al. (2010) and compared to ECHAM/MADE-in results in Fig. 5.

3 µm. The data set covers not only a very large geographical region, but also different seasons and years and is therefore well suited for a comparison with a global climate model. The simulated vertical profiles were calculated from climatological means of the months of the observations (March, May, September and November) in the grid boxes containing the measurements sites. The agreement between simulated and observed concentrations is reasonably good at all latitudes, especially in the UTLS. The deviations of the observed and simulated concentrations are mostly smaller than the corresponding variability.

The observations shown in Fig. 8a and b were taken as part of the INCA project (Minikin et al., 2003) during nine flights departing from Prestwick, Scotland, in October 2000 and ten flights from Punta Arenas, Chile, in March and April 2000. Figure 8c shows measurements from Petzold et al. (2002) during the LACE campaign, which took place over the area of Berlin, Germany (13.5°–14.5° E, 51.5°–52.7° N) in August 1998. Since the aerosol concentrations were measured only during the takeoff and landing phase of the flights, the simulated profiles were derived for the grid

Fig. 7. Vertical profiles of the mean aerosol number concentration (converted to STP conditions: 273 K, 1013 hPa) from measurements by Clarke and Kapustin (2002) taken with an UCN counter over the Pacific Ocean and corresponding model values. For clarity, only positive standard deviations are shown.
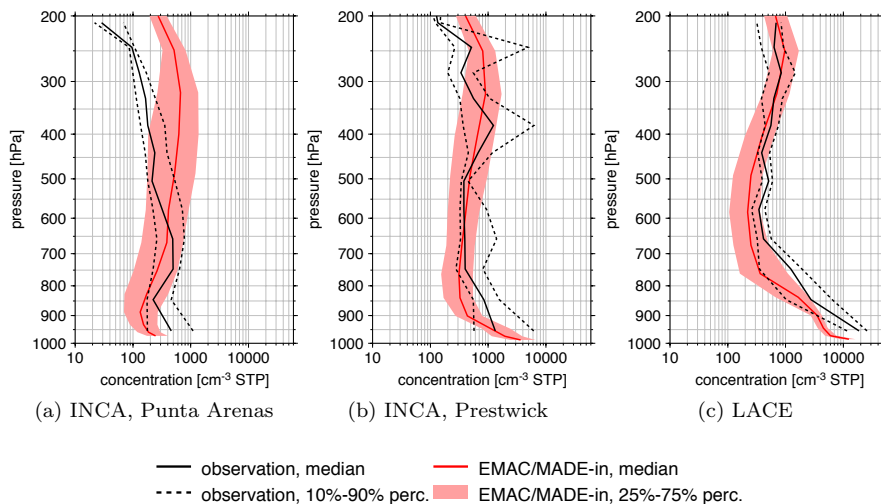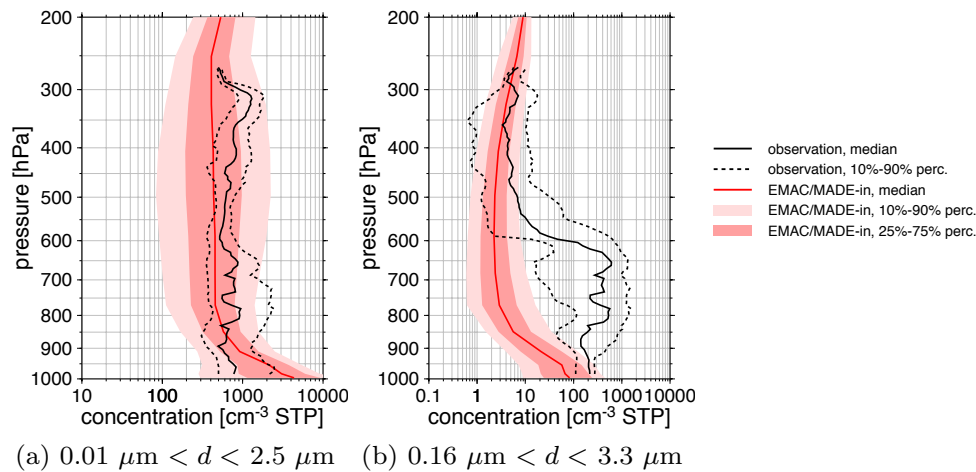

Fig. 8. Vertical profiles of the number concentration (converted to STP conditions: 273 K, 1013 hPa) of aerosol particles larger than 5 nm as measured by Minikin et al. (2003) during INCA over Punta Arenas (Chile) in March-April 2000 and over Prestwick (Scotland) in October 2000 (**a** and **b**, respectively) and by Petzold et al. (2002) during LACE over central Europe in August 1998 **(c)** and corresponding model data.

box containing the airports (4.5° W, 55.5° N for Prestwick and 71.1° W, 53° S for Punta Arenas). The agreement between modeled and observed profiles is particularly good in the case of Fig. 8b and c. Figure 8a shows an overestimation of the modeled median number concentration above 600 hPa. However, the measured and simulated data agree within the 25% and 75% percentiles up to 350 hPa. The model slightly underestimates the number concentrations measured during the LACE campaign at all altitudes up to 350 hPa (Fig. 8c), but it is in very good agreement with the observations in the UTLS.

Figure 9 shows the comparison between the vertical profiles of the simulated aerosol number and measurements from Weinzierl et al. (2009) during the Saharan Mineral Dust Experiment (SAMUM). SAMUM was conducted in May/June 2006 over southern Morocco with the purpose of investigating the vertical structure of dust layers and their microphysical and chemical properties.

The flights were performed during dust storms, and the data were taken when the relative humidity was lower than 90%. The same condition on the relative humidity is imposed on the model data included in the calculation of the

(a) $0.01 \ \mu m < d < 2.5 \ \mu m$ (b) $0.16 \ \mu m < d < 3.3 \ \mu m$

Fig. 9. Vertical profiles of the aerosol number concentration (converted to STP conditions: 273 K, 1013 hPa) measured by Weinzierl et al. (2009) during SAMUM over southern Morocco in May/June 2006 and corresponding model data. Shown are the number concentrations of aerosol particles with diameters between 10 nm and 2.5 µm (**a**) and between 160 nm and 3.3 µm (**b**).

median values. In the model set-up used for this study dust emissions are not calculated online but taken from a fixed climatology. Thus, specific dust storms events cannot be simulated. However, the agreement between simulated and observed number concentration is good for the particle sizes and altitude ranges that are influenced only to a minor extent by dust storms. Simulated and observed particle number in the smallest size range are in good agreement at all altitudes (Fig. 9a). Small particles, which are mainly composed of compounds other than dust, dominate the number concentration. Thus, increases in the number of larger dust particles because of dust storms impact the total number concentration in this size range only weakly. The observed profile in Fig. 9b shows a layer up to 600 hPa where the number concentration of large particles is much higher than in the layer above. Weinzierl et al. (2009) concluded that the dust risen by the storm is confined to the lower troposphere because of the prevailing meteorological conditions. The simulated concentrations agree with the unperturbed observed concentration above 600 hPa, but, as expected, EMAC/MADE-in cannot reproduce the concentrations perturbed by the dust storm.
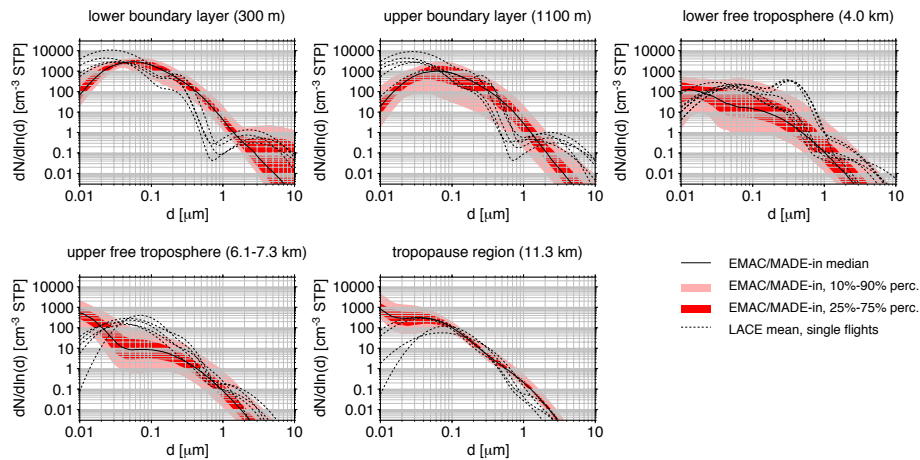
3.3 Aerosol size distribution

Figure 10 shows a comparison of the modeled and observed size distributions at different altitudes during the LACE field campaign (Petzold et al., 2002). Overall, the agreement between the two data sets is reasonably good. However, some discrepancies are apparent. In the boundary layer and in the lower free troposphere (around 4 km altitude) the experimental data show a clear trimodal behavior, with a coarse mode consisting of particles larger than 1 µm. This behavior is not well reproduced by EMAC/MADE-in. A possible reason is

that the simulated coarse mode includes only aerosol water, sea salt and mineral dust from natural sources. Coarse mode dust can also be generated by human activities and can possibly have a large contribution, particularly over continents in the northern hemisphere. However, in the lower boundary layer the observed coarse mode is within the variability of the model.

Above 6 km altitude the model overestimates the number of particles with diameters smaller than 0.02 µm and underestimates the number of larger particles, while the total number concentration is represented well (Fig. 8). This is probably due to nucleation of small SO_4 particles, which becomes more important with increasing altitude. EMAC/MADE-in assigns the freshly nucleated particles to the soluble Aitken mode. Since the standard deviations of the MADE-in modes are fixed, a large injection of very small particles shifts the whole size distribution towards smaller diameters. An improvement of the modeled aerosol size distributions could possibly be achieved by adding a separate nucleation mode. It has also to be noted that particle nucleation is a highly variable process in the UTLS. During the LACE study, aerosol nucleation was investigated in detail by Schröder et al. (2002). The observed number concentrations in the free troposphere ranged from 10 particles cm^{-3} to 4000 particles cm^{-3} depending on the properties of the accumulation mode aerosol. This short-scale variability is beyond the resolution of global models.

Figure 11 shows the comparison of the simulated aerosol size distribution at surface level with the observations by Birmili et al. (2001) in Melpitz, central Germany (51°32′ N, 12°56′ E), for different air masses and weather conditions obtained between March 1996 and August 1997. The observation site is far from major cities, therefore the observed

Fig. 10. Aerosol number size distributions at different altitudes measured by Petzold et al. (2002) during the LACE campaign over central Europe in August 1998 and corresponding simulated size distributions. Particle diameters correspond to dry aerosol.
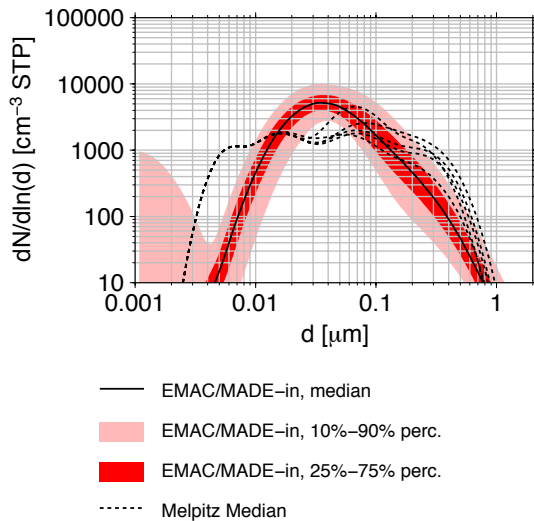
Fig. 11. Aerosol number size distributions at surface level as observed by Birmili et al. (2001) in the region of Melpitz, Germany, and corresponding model values. The dashed lines show the size distributions for different air masses and weather conditions. The simulated number size distribution is a climatological median of 10 yr and refers to the dry diameter.

size distribution is rather typical for rural conditions. The model grid box considered in this comparison spans between 50.23° N and 53.50° N and between 9.84° E and 12.66° E. Since such a large area includes also polluted areas, the simulated number size distribution does not correspond completely to rural conditions. This may explain the higher number concentrations simulated by EMAC/MADE-in, as well as the Aitken mode with very small diameters shown by the 90% percentile line and caused by nucleation of H_2SO_4 va-

por. The simulated size range and the order of magnitude of the median number concentration are in agreement with the observations. Again, the introduction of an additional nucleation mode in MADE-in could probably lead to a better agreement with the data by Birmili et al. (2001) for particles smaller than 10 nm.

The simulated aerosol number size distributions are also compared with aerosol measurements collected by Putaud et al. (2002). The observations were taken at different sites in Europe during winter (Fig. 12) and during summer (Fig. 13). As noted for Fig. 11, also in this case none of the model grid boxes represents purely rural or urban conditions. We therefore expect higher simulated aerosol concentrations at measurement sites characterized by rural conditions and lower concentrations at urban sites due to the presence of both cities and rural areas in the same model box. This expectation is confirmed at all sites. Taking this into account, EMAC/MADE-in agrees reasonably well with the observed number size distributions. As for the comparison with the size distributions from Petzold et al. (2002) (Fig. 10) and Birmili et al. (2001) (Fig. 11), the simulated Aitken mode often shows too high number concentrations for particle diameters smaller than 5 nm, especially in urban areas and in summer, when the larger insolation favors the formation of SO_4. This could be related to a too effective nucleation process in the model.

3.4 Mixing state of black carbon particles

Not many measurement techniques are capable of resolving the mixing state of insoluble particles. Schwarz et al. (2008) presented data taken during the CR-AVE campaign with the SP2 instrument, showing the BC number fraction contributed by internally mixed BC particles. The comparison between simulated and observed BC mixing state is complicated for
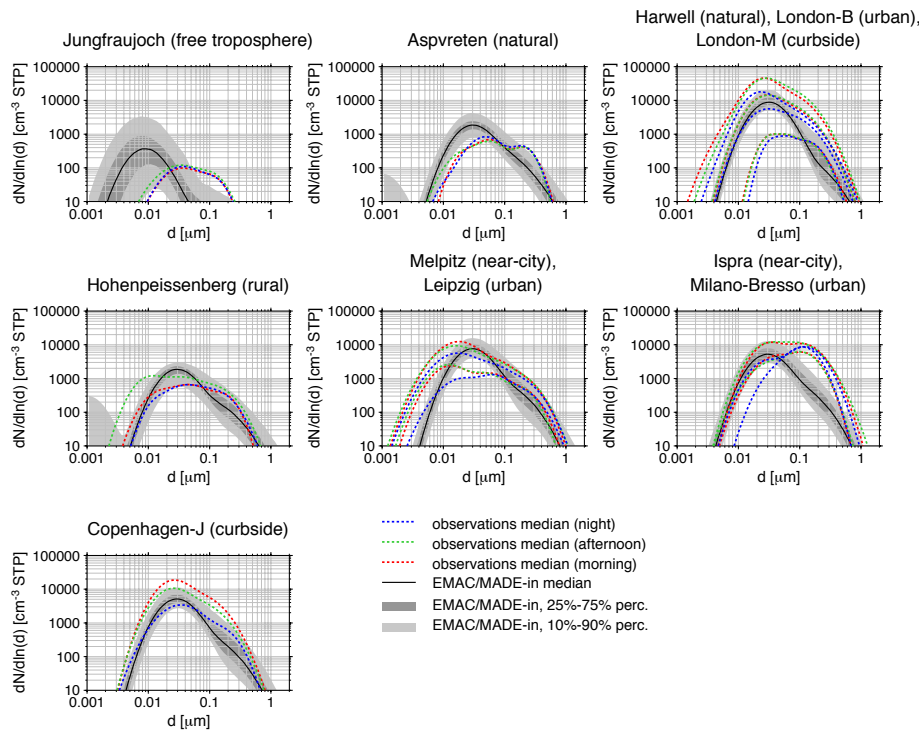
Fig. 12. Aerosol number size distributions at surface level as observed at different sites in Europe (Putaud et al., 2002) during winter (December, January, February) and corresponding model size distributions. The observed size distributions are three-modal log-normal distributions fitted to the measurements data. The simulated number size distributions are climatological medians of 10 yr calculated for the location and months of the observations.
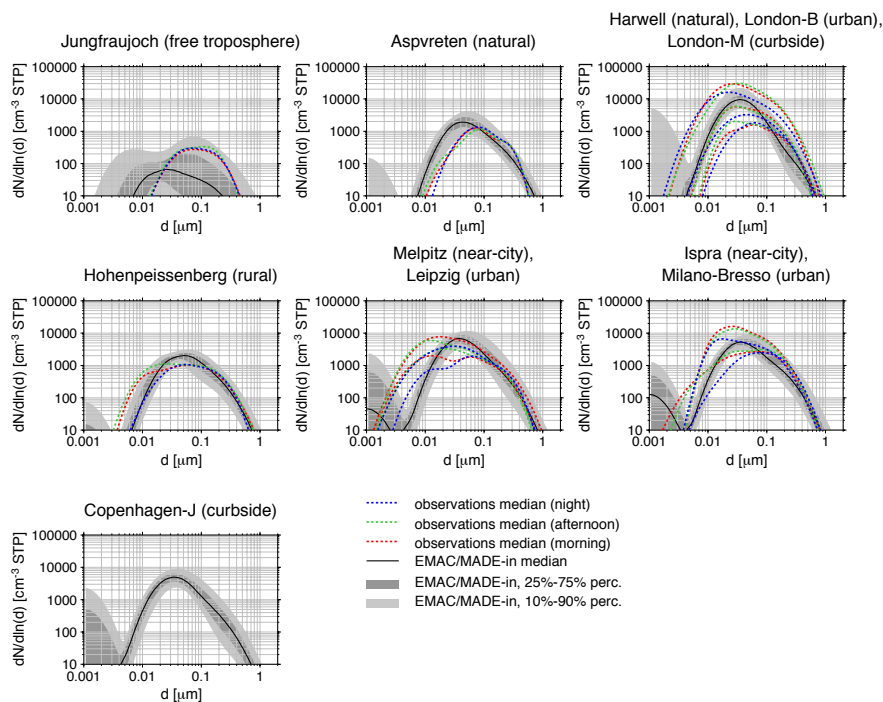

Fig. 13. As Fig. 12 but for summer (June, July, August). No measurements at the Copenhagen site are available.

several reasons. First, the SP2's ability to detect the presence of internally mixed mass associated with a BC core depends on the mass of the BC component. Quantification of this ability requires the adoptions of several assumptions as refractive index and density and the use of Mie theory, modeling the particles as concentric coated spheres. Hence this ability is not well-characterized (Schwarz et al., 2008). Second, the mixing state of BC particles can be determined from SP2 data only for particles with a BC core in the size range of 100–250 nm, corresponding to only a slice of the MADE-in accumulation mode. Discrepancies in the simulated and observed concentration within a particle size window could originate from a shift in the particle median diameter, and not by a lack of particles. Furthermore, the SP2 size window refers to the size of the BC cores, while the size distributions simulated by MADE-in refer to the size of whole particles, composed of core and coating. Comparing only the mixing state of the simulated accumulation mode would not be correct, since it contains also particles with BC cores outside the SP2 detection window. Moreover, MADE-in simulates the number concentration of insoluble particles, therefore the simulated number concentration in the accumulation mode includes also the number concentration of dust particles.

To allow at least for a qualitative comparison, a simulation has been performed where neither dust nor Aitken mode BC particles are emitted. In this test the insoluble aerosol is composed only of BC particles that are of similar size as the ones detected by SP2. This comparison cannot be quantitative, since the aerosol population generated in such a simulation is not fully realistic. Consequently, the formation of clouds, the aerosol effect on radiation and even the aging of accumulation mode BC could be different. However, it can help to understand whether the simulation of the aging process is effective enough. In this simulation (BCACC90) the critical fraction of soluble material needed to define a BC particle as internally mixed is set to 90%, which is an estimate of the upper limit on the amount needed by the SP2 to detect a coating (J. Schwarz, personal communication, 2008). However, this is probably in most cases a more sensitive identification of internal mixture than that performed by the SP2. To check the sensitivity of this comparison to the choice of the threshold for internal mixing, we perform the same test with critical fractions of 10% (BCACC10), 50% (BCACC50) and 80% (BCACC80). Each simulation is performed over a 5-yr period after a 1-yr spin-up. We find that the vertical profiles of the number fraction of internally mixed BC particles are not very sensitive to these changes.

Figure 14 shows the vertical profile of the mean soluble mass fraction in the internally mixed BC modes, calculated for the reference simulation (REF) evaluated in this work (critical fraction equal to 10% and complete set of emissions) along the flight performed by Schwarz et al. (2008). The soluble mass represents more than 85% of the total mass of the mode along the whole vertical profile. This implies that the aging processes are fast and lead to large average coatings.
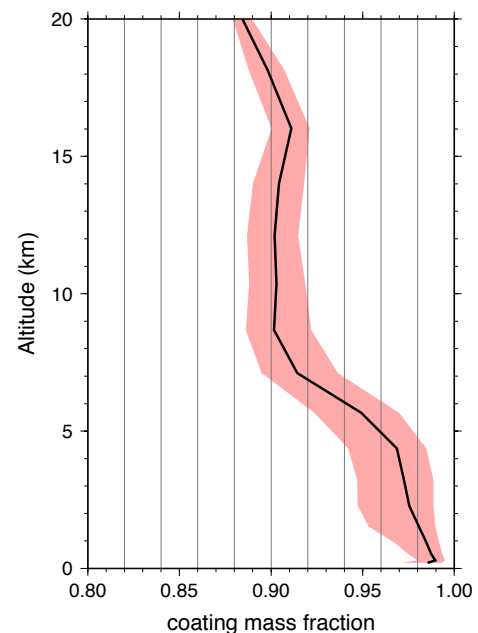
Fig. 14. Vertical profile of the mean soluble mass fraction in the internally mixed modes with BC and dust (akn_{mix} and acc_{mix}) calculated from the reference simulation REF along the routes of flights performed by Schwarz et al. (2008). The thick solid line represent the median values and the shaded areas are defined by the 25% and 75% percentiles.

Figure 15 shows the number fraction of internally mixed BC in the simulation BCACC90. As Schwarz et al. (2008) concluded from their observations, large fractions of BC particles in the UTLS are internally mixed. EMAC/MADE-in simulates that between 85% and 95% of UTLS BC particles are internally mixed, while Schwarz et al. (2008) find fractions between 60% and 80% with values of higher statistical significance being closer to 80%. Up to 5 km altitude the fraction of internally mixed BC particles calculated from SP2 measurements scatters over a large range of values between 20% and 70%. This is probably related to the variability of the sources and history since emission, impacting particularly lower altitudes. Between 5 km and 15 km the SP2 number fractions of internally mixed BC stay below 50%, where, however, the statistical uncertainty of the values is high due to the low number of BC particles detected. Only above 15 km the fraction increases with altitude. The simulated number fraction, on the other hand, stays relatively constant with altitude. This suggests that BC ages already at lower levels in the model. The emissions of BC in EMAC/MADE-in over the CR-AVE area are generally low. A large amount of BC may have been transported from other regions and become internally mixed during the transport. The fraction of internally mixed BC particles is indeed lower over the major BC emissions areas. Over central Africa, a
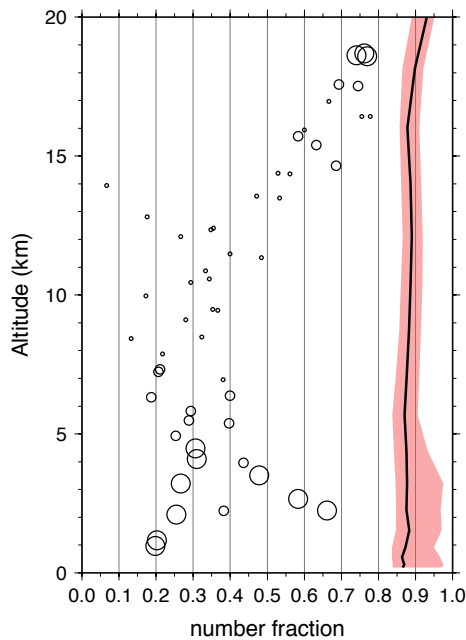
Fig. 15. Number fraction of internally mixed BC particles as calculated by Schwarz et al. (2008) from observations taken during the CR-AVE campaign (open circles) and as simulated by EMAC/MADE-in (shaded area) in the simulation BCACC90. The solid line is the median value and the shaded areas are defined by the 10% and 90% percentiles. Each open circle corresponds to a 1-km average from one flight with the symbol diameter roughly proportional to its statistical confidence; large, medium, and small symbols correspond to <5%, <10%, and <25% statistical uncertainty, respectively.

region characterized by strong forest fires, the fraction of internally mixed BC particles in simulation BCACC90 is equal to 80% in the boundary layer. The results of the reference run (REF) show that 96% of BC particles are internally mixed at surface level over the CR-AVE region, 73% over central Africa and 61% over the New York City area, which is characterized by high emission rates of anthropogenic BC. While the BC emissions in central Africa contribute mainly to the accumulation mode, those over New York City mainly contribute to the Aitken mode. These values are summarized in Table 6.

Pratt and Prather (2010) have published experimental data of the number fraction of internally mixed BC between 1 km to 6 km altitude during the ICE-L campaign performed over Wyoming, western Nebraska, southwestern South Dakota and northern Colorado during November and December 2007. They use a mass spectrometer technique detecting internal mixtures in a different way than both the model and the SP2. They detected number fractions of particles containing internally mixed elemental and organic carbon between 62% and 77%. These values are on the upper end of those calculated by Schwarz et al. (2008). EMAC/MADE-

Table 6. Number fraction of internally mixed BC at surface level in the simulations REF and BCACC90 over the region of the CR-AVE campaign, central Africa and the New York City area. These three regions are characterized by low BC emissions, biomass burning (accumulation mode BC) and anthropogenic emissions (Aitken mode BC), respectively. No value is given for BCACC90 over New York City since BCACC90 does not account for Aitken mode BC emissions.

	CR-AVE	Central Africa	New York city
REF	96%	73%	61%
BCACC90	86%	80%	–

in simulates fractions of internally mixed particles between 84% and 95% over the area investigated by Pratt and Prather (2010) (run BCACC90). These comparisons suggest that the efficiency of the aging process of insoluble particles as represented in the current version of the model may be comparatively high. In the global model studies by Bauer et al. (2008) and Lohmann and Hoose (2009) similar representations of BC aging as applied here were considered. Also these models tend to simulate higher fractions of internally mixed BC as suggested by the observations. This reveals that the BC aging as currently represented in these models may be too efficient. However, this conclusion should be carefully considered, given the uncertainties inherent in the measurements and possible systematic differences caused by limitations in the comparability of the model results and the observations. To assess possible uncertainties in the model representation of insoluble particle aging, further research is necessary applying also alternative methods to simulate the aging process.

3.5 Comparison with global aerosol models

SO_4 has a large contribution to the total aerosol mass in the sub-micrometer range. The average global burden of SO_4 simulated by EMAC/MADE-in is 1.5 Tg, followed by POM (0.8 Tg), NH_4 (0.4 Tg), dust (0.2 Tg in the accumulation modes, 9.0 Tg if the coarse mode dust is included), NO_3 (0.1 Tg), sea salt (0.1 Tg in the accumulation modes, 2.5 Tg including the coarse mode) and BC (0.1 Tg). As shown in Table 7, these burdens are consistent with those modeled by EMAC/MADE (Lauer et al., 2007) and by, except for sea salt, ECHAM5/HAM (Stier et al., 2005; Kloster et al., 2008), which is also based on the ECHAM general circulation model. Textor et al. (2007) present an assessment of global burdens of SO_4, POM, dust, sea salt and BC from different global aerosol models participating in the AeroCom project. They calculated global mean burdens of $2.1\pm25\%$ Tg for SO_4, $1.3\pm18\%$ Tg for POM, $0.2\pm26\%$ Tg for BC, $21.3\pm21\%$ Tg for dust (including coarse mode) and $12.7\pm31\%$ Tg for sea salt (also including the coarse mode). While BC in EMAC/MADE-in is still within the range of the AeroCom inter-model variability, the burdens of sulfate

Table 7. Global aerosol burden simulated by EMAC/MADE-in, EMAC/MADE (Lauer et al., 2007), ECHAM5/HAM (Stier et al., 2005; Kloster et al., 2008) and from multi-model means compiled by the AeroCom aerosol model intercomparison initiative (Textor et al., 2007) in Tg.

| Species	EMAC/ MADE-in	EMAC/ MADE	ECHAM5-HAM	AeroCom
SO_4	1.5	1.5	0.8	2.1 ± 0.5
BC	0.1	0.1	0.1	0.2 ± 0.1
POM	0.8	1.1	1.0	1.3 ± 0.2
SS	2.5	3.6	10.5	12.7 ± 3.9
DU	9.0	9.0	8.3	21.3 ± 4.5
NH_4	0.4	0.4	–	–
NO_3	0.1	0.1	–	–

and POM are lower than those indicated by Textor et al. (2007). SO_4 originates predominantly from oxidation of precursor gases, therefore discrepancies in its burden may be related to different parameterization of the sulfur cycle in the chemistry module. This might also explain the discrepancy in the SO_4 burden simulated by EMAC/MADE-in and ECHAM5/HAM. The lower POM burden of EMAC/MADE-in could be due to a more effective scavenging. As for BC (Sect. 2.2), EMAC/MADE assumes an exponential decay from hydrophobic to hydrophilic POM with e-folding time of one day. EMAC/MADE-in assumes the same for the POM in the soluble modes akn_{sol} and acc_{sol}, but considers all POM in the coating of internally mixed BC and dust particles (akn_{mix} and acc_{mix} modes) as hydrophilic. Compared to EMAC/MADE, EMAC/MADE-in simulates more hydrophilic POM, thus more POM in EMAC/MADE-in than in EMAC/MADE will be removed by nucleation scavenging and subsequent wet deposition. In the case of dust, EMAC/MADE-in considers the same emissions as Aero-Com. The dust burden simulated by EMAC/MADE-in is at the lower end of the range simulated by the AeroCom models. Since this is also the case for the ECHAM5/HAM dust burden, it could be related to general features of the ECHAM model family, such as transport characteristics, rather than specific properties of MADE-in. As discussed in Sect. 3.1, the lower burden could also be due to the splitting between accumulation and coarse mode or to an overestimation of coarse mode sinks. Also the total burden of sea salt simulated by EMAC/MADE-in and EMAC/MADE is particularly smaller compared to the AeroCom mean. The same consideration as for dust may apply to sea salt, since sea salt and dust are the two aerosol species included in the coarse mode. However, the comparability of sea salt values is limited since sea salt emissions are calculated online from the simulated winds in EMAC, while an emission climatology of the year 2000 was used for the AeroCom simulations.

4 Predicting the number concentration of insoluble particles with EMAC/MADE-in

Due to its specific features and its performance, EMAC/MADE-in is a well suited tool for studying the global distribution and properties of insoluble particles in the atmosphere. Figure 16 shows an example for a possible application of EMAC/MADE-in. Shown is the horizontal distribution at 300 hPa and the vertical distribution of the zonal mean number concentration (climatological annual means) of particles containing BC and/or dust and their mixing state. Their number concentration is calculated as the sum of the number concentration of the akn_{mix}, acc_{mix}, akn_{ext} and acc_{ext} modes (Fig. 16a). While at surface level (not shown) the horizontal distribution of insoluble particles is strongly influenced by the location of the sources, the geographic patterns are more homogeneous at 300 hPa. However, the plumes of strong emission areas as China and North America can be clearly identified.

Figure 16b shows the fraction of the total aerosol number concentration that contains BC or dust. Around 300 hPa only up to 1% of the total aerosol contains dust or BC. This is in agreement with Sheridan et al. (1994), who found that fewer than 1% of the particles in the upper troposphere contain soot. The highest values are reached over emission areas that experience strong convection, which can move insoluble particles from the surface to 300 hPa in a relatively short time. Their number fraction decreases with altitude up to 200 hPa (right panel). The minimum occurs around the tropopause, where very efficient nucleation increases the number concentration of soluble aerosol. Note that no BC emissions from aircraft are included in this simulation. Hendricks et al. (2004) found by means of global simulations with a mass-based aerosol module that the amount of BC from aviation at 250 hPa (main flight level) could represent only a few percent of the total large-scale mean BC mass. The highest contributions were found over Europe and within the North Atlantic flight corridor. A corresponding estimate of the number contribution based on prescribed size distributions, suggests that BC particles from aircraft could contribute up to 30% to the total BC particle number concentration, noticeably increasing the number concentration of insoluble particles in the UTLS. Hendricks et al. (2004) considered emission data representative for the years around 1990. An update of these results by consideration of BC from aviation in EMAC/MADE-in could be a subject of future research.

Figure 16c shows the mixing state of insoluble particles in the atmosphere. Even though 80% of BC and 100% of dust are emitted as externally mixed, most of the insoluble particles have undergone an aging process and have been transferred to an internal mixture. The zonal mean shows higher number fractions of externally mixed BC and dust particles over the equator. This is probably due to the fast updraft that moves relatively fresh air to high altitudes. A second maximum is reached at 60° N latitude at around 500 hPa. This
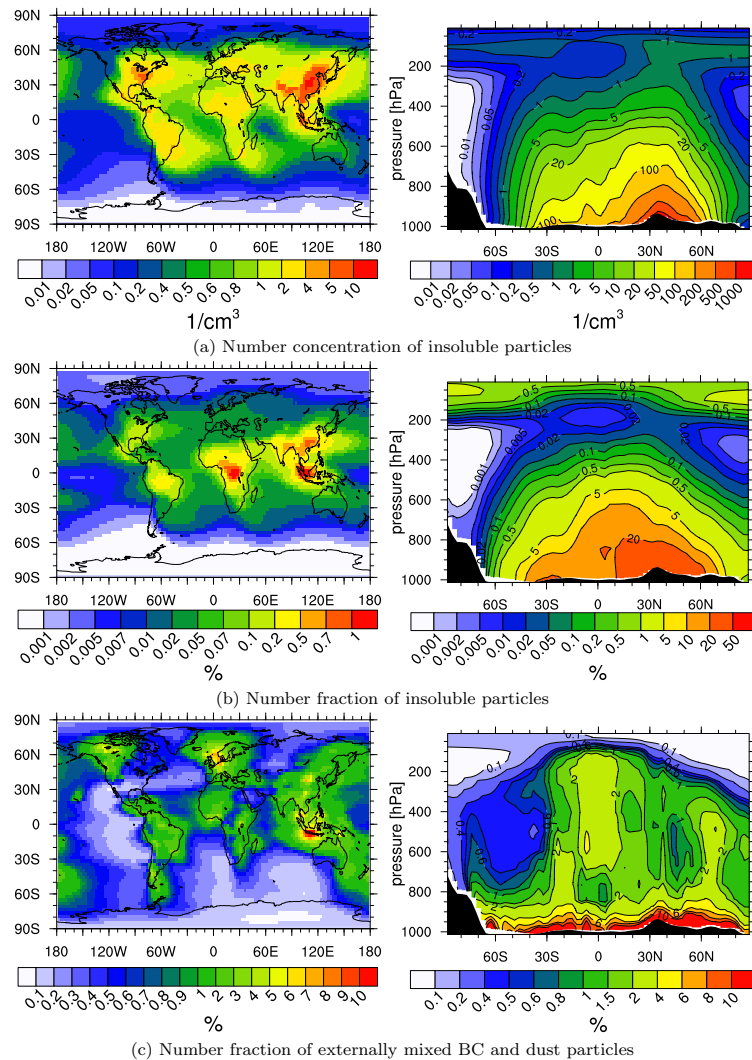
Fig. 16. Annual means of the horizontal global distribution at 300 hPa (left) and zonal mean vertical distribution (right) of **(a)** the number concentration of insoluble particles, **(b)** the number fraction of insoluble particles, and **(c)** the contribution of externally mixed BC and dust particles to their total number.

spot with a high concentration of externally mixed BC is related to wildfires in the boreal Canada, which are assumed to reach 6 km altitude by the model (Dentener et al., 2006).

5 Conclusions

The newly developed aerosol-climate model EMAC/MADE-in is able to resolve number and mixing state of BC and dust particles and to keep track of the number of BC and dust free particles. The aerosol microphysics model MADE-in describes the aerosol distribution as a superposition of seven log-normal modes: two modes (an Aitken and an accumulation mode) are dedicated to BC and dust without or with only a small amount of soluble material, two modes to par-

ticles containing BC, dust and other soluble species, two to BC and dust free particles, and one coarse mode to particles composed of dust, sea salt and water. The processes simulated by MADE-in are condensation of H_2SO_4 and organic vapors, binary nucleation of sulfuric acid and water vapor, coagulation of particles and partitioning between the gas and particulate phase of water, nitric acid and ammonia. MADE-in calculates the evolution of the number concentrations of the seven modes and of the mass concentrations of the individual species in each mode.

MADE-in is implemented in the global ECHAM/MESSy Atmospheric Chemistry (EMAC) model, which simulates the emission of particles and particle precursors, their atmospheric dispersion, chemical transformation and dry and wet removal. In the set-up used for the simulations presented in

this work, chemistry and aerosol are coupled through DMS and SO_2 oxidation as well as particle uptake of HNO_3 and NH_3 from the gas phase. The aerosol distributions calculated by MADE-in are used in the calculation of the radiative fluxes and of the concentration of cloud droplets. The model system has been evaluated with surface and airborne measurements of aerosol mass and number concentrations and size distributions. The model mostly agrees well with observations. The comparison suggests an overestimation of the simulated number concentration of very fine particles with diameters of some nanometers. An improved representation of such small particles by adding a separate nucleation mode should be aimed at in future studies. The concentrations of dust and sea salt particles in the lower troposphere appear to be underestimated. Further studies are required to identify the reasons for such discrepancies. We plan to apply MADE-in in simulations of aerosol-induced cirrus formation, taking into account possible effects of BC from aircraft on cirrus. Therefore, we devoted our efforts to obtain a reliable simulation of the UTLS, especially regarding BC particles. The vertical profiles of aerosol concentrations have shown that the model performs particularly well in that region.

EMAC/MADE-in also allows for detailed studies on aging of BC and dust particles. The contributions of cloud processing, coagulation and condensation to the aging of BC and dust are modeled separately. Model experiments can be performed where specific aging processes can be neglected. Such simulations can be used to estimate the relative importance of the individual aging processes. Furthermore, the consideration of different modes for different mixing states of BC and dust enables the calculation of the typical time scales of BC to gain a soluble coating, which is arbitrarily assumed to be around one or two days in many global aerosol models. Such studies can be subject of future publications.

Appendix A

Calculation of the condensation coefficients

A1 Condensation of sulfuric acid

The mass concentration of sulfuric acid gas evolves following the analytic solution of the equation

$$\frac{dC_{H_2SO_4}(t)}{dt} = P - L \cdot C_{H_2SO_4}(t), \quad (A1)$$

where P is the production rate of H_2SO_4 in the gas phase, which is provided by the gas phase chemistry scheme to the aerosol submodel, and L is the loss due to condensation. The solution of Eq. (A1) is

$$C_{H_2SO_4}(t) = \frac{P}{L} + \left(C_{H_2SO_4}(t_0) - \frac{P}{L}\right)e^{-L(t-t_0)}, \quad (A2)$$

assuming that P and L are constant during $\Delta t = t - t_0$. The change in the mass concentration of H_2SO_4 due to the contribution of condensation ($\Delta C^{cond.}$) is

$$\Delta C^{cond.} = \Delta C_{H_2SO_4} - \Delta C^{production}$$
$$= \left(\frac{P}{L} - C_{H_2SO_4}(t_0)\right)(1 - e^{-L\Delta t}) - P\Delta t. \quad (A3)$$

The loss coefficient L is calculated following Whitby et al. (1991). The loss of H_2SO_4 in the gas phase is equal to the gain of SO_4^{2-} mass in the aerosol modes. If $M_i^{(k)}$ is the kth moment of the mode i and $G_i^{(k)}$ the corresponding growth coefficient, we have:

$$L = \sum_{i=1}^{N_{modes}} \frac{\partial C_{SO_4^{2-},i}}{\partial t} = \rho_{SO_4} \frac{\pi}{6} \sum_{i=1}^{N_{modes}} \frac{\partial M_i^{(3)}}{\partial t} \quad (A4)$$
$$\equiv \rho_{SO_4} \frac{\pi}{6} \sum_{i=1}^{N_{modes}} G_i^{(3)},$$

where the relation between mass and third moment from Eq. (4) is used. ρ_{SO_4} is the specific density of particulate SO_4. $G_i^{(3)}$ can be factorized in a size-dependent factor $\Psi(D)$, where D is the particle diameter, and in a size-independent factor Ψ_T (Whitby and McMurry, 1997):

$$G_i^{(3)} = \frac{6}{\pi} \Psi_T \int_0^\infty \Psi(D) n_i(D) dD. \quad (A5)$$

The size-independent component Ψ_T of the growth function is equal to

$$\Psi_T = \frac{M_w p_s (S_v - 1)}{\rho R T} \quad (A6)$$

where M_w is the molecular weight of the condensing gas, p_s the saturation vapour pressure, S_v the saturation ratio of the condensing species, ρ the density of the condensed substance, R the universal gas constant and T the temperature. The form of the size-dependent component $\Psi(D)$ depends on the regime of the gas, which is identified by the Knudsen number Kn. $\Psi(D)$ has two asymptotic forms for the free molecular ($Kn > 10$) and near continuum ($Kn < 1$) regimes:

$$\text{free-molecular:} \quad Kn > 10: \Psi^{fm}(D) = \frac{\pi \alpha \bar{c}}{4} D^2 \quad (A7)$$

$$\text{near-continuum:} \quad Kn < 1: \Psi^{nc}(D) = 2\pi D_v D \quad (A8)$$

where α is the accomodation coefficient, $\bar{c}$ the mean molecular velocity and D_v the diffusion coefficient. The asymptotic expressions for the growth rate are:

$$G_i^{(3)fm} = \frac{6}{\pi} \Psi_T \frac{\pi \alpha \bar{c}}{4} M_i^{(2)} \quad (A9)$$

$$G_i^{(3)nc} = \frac{6}{\pi} \Psi_T 2\pi D_v M_i^{(1)}. \quad (A10)$$

Whitby et al. (1991) showed that the harmonic mean between the free-molecular and the near-continuum expressions gives an expression of the growth rate that is computationally efficient and precise enough also in the transition between the two regimes:

$$G_i^{(3)} = \frac{G_i^{(3)fm} G_i^{(3)nc}}{G_i^{(3)fm} + G_i^{(3)nc}}. \tag{A11}$$

The loss coefficient L is calculated substituting Eq. (A11) in Eq. A4. The growth of SO$_4$ mass concentration in each mode i due to condensation of sulfuric acid ($\left.\frac{\partial C_{x,i}}{\partial t}\right|_{\text{cond}}$ in Eq. 8) is calculated through the non-dimensional coefficients Ω_i:

$$\left.\frac{\partial C_{\text{SO}_4^{2-},i}}{\partial t}\right|^{\text{cond}} = \Omega_i \Delta C^{\text{cond}}. \tag{A12}$$

$$\Omega_i = \frac{G_i^{(3)}}{\sum_{i=1}^{N_{\text{modes}}} G_i^{(3)}}. \tag{A13}$$

A2 Condensation of organic gases

The condensation of organic gases into secondary organic aerosol is calculated analogously to the condensation of sulfuric acid. The amount of condensing gas C_{SOA}, however, is not calculated, but prescribed using effective emissions of condensable organic gases from Dentener et al. (2006). Therefore

$$\left.\frac{\partial C_{\text{POM},i}}{\partial t}\right|^{\text{cond}} = \Omega_i^{\text{SOA}} C_{\text{SOA}} \tag{A14}$$

$$\Omega_i^{\text{SOA}} = \frac{G_{\text{SOA},i}^{(3)}}{\sum_{i=1}^{N_{\text{modes}}} G_{\text{SOA},i}^{(3)}}. \tag{A15}$$

Appendix B

Calculation of the coagulation rate

In the case of intermodal coagulation of two particles of modes i and j to create a particle of mode l, the rate at which the kth moment of mode l increases is equal to

$$C_{k,ij}{}^l = \frac{\partial M_l^{(k)}}{\partial t} = +\int_0^\infty \int_0^\infty (D_1^3 + D_2^3)^{k/3} \tag{B1}$$
$$\beta(D_1, D_2) n_i(D_1) n_j(D_2) dD_1 dD_2,$$

following Binkowski and Shankar (1995). D_1 and D_2 are the diameters of the coagulating particles, $n_i(D)$ and $n_j(D)$ the number distributions of the modes i and j and $\beta(D_1, D_2)$ the coagulation coefficient, which depends on the regime of the

gas (see below). The moment loss rate of the modes i and j is equal to

$$C_{k,ij}{}^i = \frac{\partial M_i^{(k)}}{\partial t} = -\int_0^\infty \int_0^\infty D_1^k \tag{B2}$$
$$\beta(D_1, D_2) n_i(D_1) n_j(D_2) dD_1 dD_2,$$

$$C_{k,ij}{}^j = \frac{\partial M_j^{(k)}}{\partial t} = -\int_0^\infty \int_0^\infty D_2^k \tag{B3}$$
$$\beta(D_1, D_2) n_i(D_1) n_j(D_2) dD_1 dD_2,$$

respectively. Note that in some cases (Table 3) l can be equal to i or to j. In such cases, the effective change of momentum of mode l is the sum of Eq. (B1) and Eq. (B2), or of Eq. (B1) and Eq. (B3), respectively.

The rate of change of the kth moment of a mode i due to intramodal coagulation is

$$C_{k,ii} = \frac{1}{2} \int_0^\infty \int_0^\infty (D_1^3 + D_2^3)^{k/3} \tag{B4}$$
$$\beta(D_1, D_2) n_i(D_1) n_i(D_2) dD_1 dD_2$$
$$- \int_0^\infty \int_0^\infty D_1^k$$
$$\beta(D_1, D_2) n_i(D_1) n_i(D_2) dD_1 dD_2.$$

In the case of intramodal coagulation, the total particle volume of the mode is not affected. The asymptotic expressions of $\beta(D_1, D_2)$ for the free-molecular ($Kn > 10$) and near-continuum ($Kn < 1$) regimes are, following Friedlander (2000),

$$\beta^{fm}(D_1, D_2) = \sqrt{\frac{3k_B T}{\rho}\left(\frac{1}{D_1^3} + \frac{1}{D_2^3}\right)}(D_1 + D_2)^2 \tag{B5}$$

$$\beta^{nc}(D_1, D_2) = 2\pi(D_{v,1} + D_{v,2})(D_1 + D_2) \tag{B6}$$

where k_B is the Boltzmann constant, T the temperature, ρ the particle density and $D_{v,i}$ the diffusion coefficient of the particle i. As done for the calculation of the condensation coefficients (Appendix A), the coagulation rates are calculated as the harmonic means of the two asymptotic regimes

$$C_{k,ij} = \frac{C_{k,ij}^{fm} C_{k,ij}^{nc}}{C_{k,ij}^{fm} + C_{k,ij}^{nc}}, \tag{B7}$$

$$C_{k,ii} = \frac{C_{k,ii}^{fm} C_{k,ii}^{nc}}{C_{k,ii}^{fm} + C_{k,ii}^{nc}}. \tag{B8}$$

Supplementary material related to this article is available online at: http://www.geosci-model-dev.net/4/325/2011/ gmd-4-325-2011-supplement.zip.

Edited by: O. Boucher

References

Abdul-Razzak, H. and Ghan, S.: A parameterization of aerosol activation, 2. Multiple aerosol types, J. Geophys. Res., 105(D5), 6837–6844, 2000.

Ackermann, I., Hass, H., Memmesheimer, M., Ebel, A., Binkowsky, F., and Shankar, U.: Modal aerosol dynamics model for Europe: development and first applications, Atmos. Environ., 32, 2971–2999, doi:10.1016/S1352-2310(98)00006-5, 1998.

Adams, P. J. and Seinfeld, J. H.: Predicting global aerosol size distributions in general circulation models, J. Geophys. Res., 107, 4370, doi:10.1029/2001JD001010, 2002.

Adams, P. J., Seinfeld, J. H., and Koch, D. M.: Global concentrations of tropospheric sulfate, nitrate, and ammonium aerosol simulated in a general circulation model, J. Geophys. Res., 104, 13791–13823, 1999.

Andreae, M. and Rosenfeld, D.: Aerosol-cloud-precipitation interactions. Part 1, The nature and sources of cloud-active aerosols, Earth-Sci. Rev., 89, 13–41, doi:10.1016/j.earscirev.2008.03.001, 2008.

Arimoto, R., Duce, R. A., Ray, B. J., Ellis, W. G., Cullen, J. D., and Merrill, J. T.: Trace-Elements in the Atmosphere over the North-Atlantic, J. Geophys. Res., 100, 1199–1213, 1995.

Ayash, T., Gong, S. L., Jia, C. Q., Huang, P., Zhao, T. L., and Lavoue, D.: Global modeling of multicomponent aerosol species: Aerosol optical parameters, J. Geophys. Res., 113, D12203, doi:10.1029/2007JD008968, 2008.

Bauer, S. E., Wright, D. L., Koch, D., Lewis, E. R., McGraw, R., Chang, L.-S., Schwartz, S. E., and Ruedy, R.: MATRIX (Multiconfiguration Aerosol TRacker of mIXing state): an aerosol microphysical module for global atmospheric models, Atmos. Chem. Phys., 8, 6003–6035, doi:10.5194/acp-8-6003-2008, 2008.

Baumgardner, D., Kok, G., Kraemer, M., and Weidle, F.: Meridional gradients of light absorbing carbon over northern Europe, Environ. Res. Lett., 3, 025010, doi:10.1088/1748-9326/3/2/025010, 2008.

Binkowski, F. and Roselle, S. J.: Models-3 Community Multiscale Air Quality (CMAQ) model aerosol compo-

nent, 1. Model description, J. Geophys. Res., 108, 4183, doi:10.1029/2002JD002762, 2003.

Binkowski, F. and Shankar, U.: The regional particulate matter model. Model description and preliminary results, J. Geophys. Res., 100, 26191–26206, 1995.

Birmili, W., Wiedensohler, A., Heintzenberg, J., and Lehmann, K.: Atmospheric particle number size distribution in central Europe: Statistical relations to air masses and meteorology, J. Geophys. Res., 106, 32005–32018, 2001.

Bond, T. C., Habib, G., and Bergstrom, R. W.: Limitations in the enhancement of visible light absorption due to mixing state, J. Geophys. Res., 111, D20211, doi:10.1029/2006JD007315, 2006.

Chernoff, D. I. and Bertram, A. K.: Effects of sulfate coatings on the ice nucleation properties of a biological ice nucleus and several types of minerals, J. Geophys. Res, 115, D20205, doi:10.1029/2010JD014254, 2010.

Chin, M., Rood, R. B., Lin, S.-J., Müller, J.-F., and Thompson, A. M.: Atmospheric sulfur cycle simulated in the global model GOCART: Model description and global properties, J. Geophys. Res., 105, 24671–24687, 2000.

Chung, S. H. and Seinfeld, J. H.: Global distribution and climate forcing of carbonaceous aerosols, J. Geophys. Res., 107, 4407, doi:10.1029/2001JD001397, 2002.

Clarke, A. and Kapustin, V.: A Pacific Aerosol Survey – Part 1: A Decade of Data on Production, Transport, Evolution and Mixing in the Troposphere, J. Atmos. Sci., 59, 363–382, 2002.

Cooke, W. F., Liousse, C., Cachier, H., and Feichter, J.: Construction of a $1° × 1°$ fossil fuel emission data set for carbonaceous aerosol and implementation and radiative impact in the ECHAM4 model, J. Geophys. Res., 104, 22137–22162, 1999.

Cziczo, D. J., Froyd, K. D., Gallavardin, S. J., Moehler, O., Benz, S., Saathoff, H., and Murphy, D. M.: Deactivation of ice nuclei due to atmospherically relevant surface coatings, Environ. Res. Lett., 4, 044013, doi:10.1088/1748-9326/4/4/044013, 2009.

DeBell, L. J., Gebhart, K. A., Hand, J. L., Malm, W. C., Pitchford, M. L., Schichtel, B. A., and White, W. H.: Spatial and seasonal and temporal vairability of haze and its constituents in the United States, Tech. Rep. IV, Cooperative Institute for Research in the Atmosphere, Colorado State University, 2006.

DeMott, P., Chen, Y., Kreidenweis, S. M., Rogers, D. C., and Sherman, D. E.: Ice formation by black carbon particles, Geophys. Res. Lett., 26, 2429–2432, 1999.

Dentener, F., Kinne, S., Bond, T., Boucher, O., Cofala, J., Generoso, S., Ginoux, P., Gong, S., Hoelzemann, J. J., Ito, A., Marelli, L., Penner, J. E., Putaud, J.-P., Textor, C., Schulz, M., van der Werf, G. R., and Wilson, J.: Emissions of primary aerosol and precursor gases in the years 2000 and 1750 prescribed data-sets for AeroCom, Atmos. Chem. Phys., 6, 4321–4344, doi:10.5194/acp-6-4321-2006, 2006.

Eyring, V., Köhler, H. W., van Aardenne, J., and Lauer, A.: Emissions from international shipping: 1. The last 50 years, J. Geophys. Res., 110, D17305, doi:10.1029/2004JD005619, 2005.

Forster, P., Ramaswamy, V., Artaxo, P., Berntsen, T., Betts, R., Fahey, D., Haywood, J., Lean, J., Lowe, D., Myhre, G., Nganga, J., Prinn, R., Raga, G., Schulz, M., and Dorland, R. V.: Climate Change 2007: The Physical Science Basis. Contribution of Working Group I to the Fourth Assessment Report of the Intergovernmental Panel on Climate Change, chap. Changes in Atmospheric Constituents and in Radiative Forcing, Cambridge Uni-

versity Press, Cambridge, United Kingdom and New York, NY, USA, 129–234, 2007.

Friedlander, S. K.: Smoke, dust and haze, Fundamentals of aerosol dynamics, Oxford University Press, New York, Oxford, 2nd Edn., 2000.

Ganzeveld, L. and Lelieveld, J.: Dry deposition parametrization in a chemistry general circulation model and its influence on the distribution of reactive trace gases, J. Geophys. Res., 100, 20999–21012, 1995.

Ganzeveld, L., Lelieveld, J., and Roelofs, G. J.: A dry deposition parametrization for sulfur oxides in a chemistry and general circulation model, J. Geophys. Res., 103, 5679–5694, 1998.

Ghan, J. S. and Schwartz, E. S.: Aerosol Properties and Processes, BAMS, 88, 1059–1083, 2007.

Guelle, W., Schulz, M., Balkanski, Y., and Dentener, F.: Influence of the source formulation on modeling the atmospheric global distribution of sea salt aerosol, J. Geophys. Res., 106, 27509–27524, 2001.

Haywood, J. and Boucher, O.: Estimates of the direct and indirect radiative forcing due to tropospheric aerosols: a review, R. Geophys., 38, 513–543, 2000.

Hendricks, J., Kärcher, B., Döpelheuer, A., Feichter, J., Lohmann, U., and Baumgardner, D.: Simulating the global atmospheric black carbon cycle: a revisit to the contribution of aircraft emissions, Atmos. Chem. Phys., 4, 2521–2541, doi:10.5194/acp-4-2521-2004, 2004.

Hendricks, J., Kärcher, B., Lohmann, U., and Ponater, M.: Do aircraft black carbon emission affect cirrus clouds on the global scale?, Geophys. Res. Lett., 32, L12814, doi:10.1029/2005GL022740, 2005.

Hess, M., Koepke, P., and Schult, I.: Optical properties of aerosol and clouds: The software package OPAC, B. Am. Meteorol. Soc., 79, 831–844, 1998.

Hitzenberger, R., Berner, A., Giebl, H., Drobesch, K., Kasper-Giebl, A., Loeflund, M., Urban, H., and Puxbaum, H.: Black carbon (BC) in alpine aerosols and cloud water-concentrations and scavenging efficiencies, Atmos. Environ., 35, 5135–5141, 2001.

Hoose, C., Lohmann, U., Erdin, R., and Tegen, I.: The global influence of dust mineralogical composition on heterogeneous ice nucleation in mixed-phase clouds, Environ. Res. Lett., 3, 025003, doi:10.1088/1748-9326/3/2/025003, 2008.

Huneeus, N., Schulz, M., Balkanski, Y., Griesfeller, J., Kinne, S., Prospero, J., Bauer, S., Boucher, O., Chin, M., Dentener, F., Diehl, T., Easter, R., Fillmore, D., Ghan, S., Ginoux, P., Grini, A., Horowitz, L., Koch, D., Krol, M. C., Landing, W., Liu, X., Mahowald, N., Miller, R., Morcrette, J.-J., Myhre, G., Penner, J. E., Perlwitz, J., Stier, P., Takemura, T., and Zender, C.: Global dust model intercomparison in AeroCom phase I, Atmos. Chem. Phys. Discuss., 10, 23781–23864, doi:10.5194/acpd-10-23781-2010, 2010.

Jacobson, M. Z.: A physically-based treatment of elemental carbon optics: Implications for global direct forcing of aerosols, Geophys. Res. Lett., 27, 217–220, 2000.

Jacobson, M. Z.: Strong radiative heating due to the mixing state of black carbon in atmospheric aerosol, Nature, 409, 695–697, 2001a.

Jacobson, M. Z.: GATOR-GCMM: A global- through urban-scale air pollution and weather forecast model 1, Model design and

treatment of subgrid soil, vegetation, roads, rooftops, water, sea ice, and snow, J. Geophys. Res., 106, 5385–5401, 2001b.

Jöckel, P., Sander, R., Kerkweg, A., Tost, H., and Lelieveld, J.: Technical Note: The Modular Earth Submodel System (MESSy) – a new approach towards Earth System Modeling, Atmos. Chem. Phys., 5, 433–444, doi:10.5194/acp-5-433-2005, 2005.

Jöckel, P., Tost, H., Pozzer, A., Brühl, C., Buchholz, J., Ganzeveld, L., Hoor, P., Kerkweg, A., Lawrence, M. G., Sander, R., Steil, B., Stiller, G., Tanarhte, M., Taraborrelli, D., van Aardenne, J., and Lelieveld, J.: The atmospheric chemistry general circulation model ECHAM5/MESSy1: consistent simulation of ozone from the surface to the mesosphere, Atmos. Chem. Phys., 6, 5067–5104, doi:10.5194/acp-6-5067-2006, 2006.

Kelly, J. T., Chuang, C. C., and Wexler, A. S.: Influence of dust composition on cloud droplet formation, Atmos. Environ., 41, 2904–2916, 2007.

Kerkweg, A., Buchholz, J., Ganzeveld, L., Pozzer, A., Tost, H., and Jöckel, P.: Technical Note: An implementation of the dry removal processes DRY DEPosition and SEDImentation in the Modular Earth Submodel System (MESSy), Atmos. Chem. Phys., 6, 4617–4632, doi:10.5194/acp-6-4617-2006, 2006a.

Kerkweg, A., Sander, R., Tost, H., and Jöckel, P.: Technical note: Implementation of prescribed (OFFLEM), calculated (ONLEM), and pseudo-emissions (TNUDGE) of chemical species in the Modular Earth Submodel System (MESSy), Atmos. Chem. Phys., 6, 3603–3609, doi:10.5194/acp-6-3603-2006, 2006b.

Kerkweg, A., Jöckel, P., Pozzer, A., Tost, H., Sander, R., Schulz, M., Stier, P., Vignati, E., Wilson, J., and Lelieveld, J.: Consistent simulation of bromine chemistry from the marine boundary layer to the stratosphere - Part 1: Model description, sea salt aerosols and pH, Atmos. Chem. Phys., 8, 5899–5917, doi:10.5194/acp-8-5899-2008, 2008.

Khalizov, A. F., Zhang, R., Zhang, D., Xue, H., Pagels, J., and McMurry, P. H.: Formation of highly hygroscopic soot aerosols upon internal mixing with sulfuric acid vapor, J. Geophys. Res., 114, D05208, doi:10.1029/2008JD010595, 2009.

Kloster, S., Dentener, F., Feichter, J., Raes, F., van Aardenne, J., Roeckner, E., Lohmann, U., Stier, P., and Swart, R.: Influence of future air pollution mitigation strategies on total aerosol radiative forcing, Atmos. Chem. Phys., 8, 6405–6437, doi:10.5194/acp-8-6405-2008, 2008.

Koch, D.: Transport and direct radiative forcing of carbonaceous and sulfate aerosols in the GISS GCM, J. Geophys. Res., 106, 20311–20332, 2001.

Koehler, K. A., Kreidenweis, S. M., DeMott, P. J., Petters, M. D., Prenni, A. J., and Möhler, O.: Laboratory investigations of the impact of mineral dust aerosol on cold cloud formation, Atmos. Chem. Phys., 10, 11955–11968, doi:10.5194/acp-10-11955-2010, 2010.

Köhler, I., Dameris, M., Ackermann, I., and Hass, H.: Contribution of road traffic emissions to the atmospheric black carbon burden in the mid-1990s, J. Geophys. Res., 106, 17997–18014, 2001.

Kotzick, R. and Niessner, R.: The effects of aging processes on critical supersaturation ratios of ultrafine carbon aerosols, Atmos. Environ., 33, 2669–2677, doi:10.1016/S1352-2310(98)00315-X, 1999.

Kumar, P., Nenes, A., and Sokolik, I. N.: Importance of adsorption for CCN activity and hygroscopic properties of mineral dust aerosols, Geophys. Res. Lett., 36, L24804,

doi:10.1029/2009GL040827, 2009.

Landgraf, J. and Crutzen, P.: An efficient method for online calculations of photolysis and heating rates, J. Atmos. Sci., 55, 863–878, 1998.

Lauer, A. and Hendricks, J.: Simulating aerosol microphysics with the ECHAM4/MADE GCM - Part II: Results from a first multi-annual simulation of the submicrometer aerosol, Atmos. Chem. Phys., 6, 5495–5513, doi:10.5194/acp-6-5495-2006, 2006.

Lauer, A., Hendricks, J., Ackermann, I, Schell, B., Hass, H., and Metzger, S.: Simulating aerosol microphysics with the ECHAM/MADE GCM - Part I: Model description and comparison with observations, Atmos. Chem. Phys., 5, 3251–3276, doi:10.5194/acp-5-3251-2005, 2005.

Lauer, A., Eyring, V., Hendricks, J., Jöckel, P., and Lohmann, U.: Global model simulations of the impact of ocean-going ships on aerosols, clouds, and the radiation budget, Atmos. Chem. Phys., 7, 5061–5079, doi:10.5194/acp-7-5061-2007, 2007.

Lelieveld, J., Brühl, C., Jöckel, P., Steil, B., Crutzen, P. J., Fischer, H., Giorgetta, M. A., Hoor, P., Lawrence, M. G., Sausen, R., and Tost, H.: Stratospheric dryness: model simulations and satellite observations, Atmos. Chem. Phys., 7, 1313–1332, doi:10.5194/acp-7-1313-2007, 2007.

Liousse, C., Penner, J. E., Chuang, C., Walton, J. J., Eddleman, H., and Cachier, H.: A global three-dimensional model study of carbonaceous aerosols, J. Geophys. Res., 101, 19411–19432, 1996.

Liss, P. S. and Merlivat, L.: Air-sea gas exchange rates: Introduction and synthesis, in: The Role of Air-Sea Exchange in Geochemical Cycling, edited by: Riedel, D., 113–127, P. Buat-Ménard, 1986.

Lohmann, U.: Possible aerosol effects on ice clouds via contact nucleation, J. Atmos. Sci., 59, 647–656, 2002.

Lohmann, U. and Feichter, J.: Global indirect aerosol effects: a review, Atmos. Chem. Phys., 5, 715–737, doi:10.5194/acp-5-715-2005, 2005.

Lohmann, U. and Hoose, C.: Sensitivity studies of different aerosol indirect effects in mixed-phase clouds, Atmos. Chem. Phys., 9, 8917–8934, doi:10.5194/acp-9-8917-2009, 2009.

Lohmann, U. and Kärcher, B.: First interactive simulations of cirrus clouds formed by homogeneous freezing in the ECHAM general circulation model, J. Geophys. Res., 107, 4105, doi:10.1029/2001JD000767, 2002.

Lohmann, U., Feichter, J., Chuang, C., and Penner, J.: Prediction of the number of cloud droplets in the ECHAM GCM, J. Geophys. Res., 104, 9169–9198, 1999.

Maenhaut, W., Fernandez-Jimenez, M.-T., Rajta, I., Dubtsov, S., Meixner, F. X., Andreae, M. O., Torr, S., Hargrove, J. W., Chimanga, P., and Mlambo, J.: Long-term aerosol composition measurements and source apportionment at Rukomechi, Zimbabwe, J. Aerosol Sci., 31 (Suppl. 1), 469–470, 2000a.

Maenhaut, W., Fernandez-Jimenez, M.-T., Vanderzalm, J. L., Hooper, B. M., Hooper, M. A., and Tapper, N. J.: Aerosol composition at Jabiru, Australia and impact of biomass burning, J. Aerosol Sci., 31 (Suppl. 1), 745–746, 2000b.

Matsuki, A., Schwarzenboeck, A., Venzac, H., Laj, P., Crumeyrolle, S., and Gomes, L.: Cloud processing of mineral dust: direct comparison of cloud residual and clear sky particles during AMMA aircraft campaign in summer 2006, Atmos. Chem. Phys., 10, 1057–1069, doi:10.5194/acp-10-1057-2010, 2010.

Mayer, B. and Kylling, A.: Technical note: The libRadtran software package for radiative transfer calculations – description and examples of use, Atmos. Chem. Phys., 5, 1855–1877, doi:10.5194/acp-5-1855-2005, 2005.

McFiggans, G., Artaxo, P., Baltensperger, U., Coe, H., Facchini, M. C., Feingold, G., Fuzzi, S., Gysel, M., Laaksonen, A., Lohmann, U., Mentel, T. F., Murphy, D. M., O'Dowd, C. D., Snider, J. R., and Weingartner, E.: The effect of physical and chemical aerosol properties on warm cloud droplet activation, Atmos. Chem. Phys., 6, 2593–2649, doi:10.5194/acp-6-2593-2006, 2006.

Meng, Z. and Seinfeld, J.: Time scale to achieve atmospheric gas-aerosol equilibrium for volatile species, Atmos. Environ., 30, 2889–2900, 1996.

Metzger, S., Dentener, F., Krol, M., Jeuken, A., and Lelieveld, J.: Gas/aerosol partitioning: 2. Global modeling results, J. Geophys. Res., 107(D16), doi:10.1029/2001JD001103, 2002a.

Metzger, S., Dentener, F., Pandis, S., and Lelieveld, J.: Gas/aerosol partitioning: 1. A computationally efficient model, J. Geophys. Res., 107, doi:10.1029/2001JD001102, 2002b.

Minikin, A., Petzold, A., Stroem, J., Krejci, R., Seifert, M., van Velthoven, P., Schlager, H., and Schumann, U.: Aircraft observations of the upper tropospheric fine particle aerosol in the Northern and Southern Hemispheres at midlatitudes, Geophys. Res. Lett., 30, 1503, doi:10.1029/2002GL016458, 2003.

Möhler, O., Buettner, S., Linke, C., Schnaiter, M., Saathoff, H., Stetzer, O., Wagner, R., Kraemer, M., Mangold, A., Ebert, V., and Schurath, U.: Effect of sulfuric acid coating on heterogeneous ice nucleation by soot aerosol particles., J. Geophys. Res., 110, D11210, doi:10.1029/2004JD005169, 2005.

Möhler, O., Benz, S., Saathoff, H., Schnaiter, M., Wagner, R., Schneider, J., Walter, S., Ebert, V., and Wagner, S.: The effect of organic coating on the heterogeneous ice nucleation efficiency of mineral dust aerosols, Environ. Res. Lett., 3, 025007, doi:10.1088/1748-9326/3/2/025007, 2008.

Monahan, E. C., Spiel, D. E., and Davidson, K. L.: A model of marine aerosol generation via whitecaps and wave disruption, in: Oceanic whitecaps and their role in air-sea exchange, edited by: Monahan, E. C. and Niocaill, G. M., D. Reidel, Norwell, Mass., 167–174, 1986.

Moteki, N., Kondo, Y., Miyazaki, Y., Takegawa, N., Komazaki, Y., Kurata, G., Shirai, T., Blake, D. R., Miyakawa, T., and Koike, M.: Evolution of mixing state of black carbon particles: Aircraft measurements over the western Pacific in March 2004, Geophys. Res. Lett., 34, L11803, doi:10.1029/2006GL028943, 2007.

Naoe, H., Hasegawa, S., Heintzenberg, J., Okada, K., Uchiyama, A., Zaizen, Y., Kobayashi, E., and Yamazakia, A.: State of mixture of atmospheric submicrometer black carbon particles and its effect on particulate light absorption, Atmos. Environ., 43, 1296–1301, 2009.

Niedermeier, D., Hartmann, S., Shaw, R. A., Covert, D., Mentel, T. F., Schneider, J., Poulain, L., Reitz, P., Spindler, C., Clauss, T., Kiselev, A., Hallbauer, E., Wex, H., Mildenberger, K., and Stratmann, F.: Heterogeneous freezing of droplets with immersed mineral dust particles - measurements and parameterization, Atmos. Chem. Phys., 10, 3601–3614, doi:10.5194/acp-10-3601-2010, 2010.

Nordeng, T.: Extended Versions of the Convective Parametrization Scheme at ECMWF and Their Impact on the Mean and Transient Activity of the Model in the Tropics, Tech. rep., ECMWF, 1994.

Nyanganyura, D., Maenhaut, W., Mathuthua, M., Makarau, A., and Meixner, F. X.: The chemical composition of tropospheric aerosols and their contributing sources to a continental background site in northern Zimbabwe from 1994 to 2000, Atmos. Environ., 41, 2644–2659, 2007.

Okada, K., Ikegami, M., Zaizen, Y., Tsutsumi, Y., Makino, Y., Jensen, J., and Gras, J.: Soot particles in the free troposphere over Australia, Atmos. Environ., 39, 5079–5089, 2005.

Oshima, N., Koike, M., Zhang, Y., Kondo, Y., Moteki, N., Takegawa, N., and Miyazaki, Y.: Aging of black carbon in outflow from anthropogenic sources using a mixing state resolved model: Model development and evaluation, J. Geophys. Res., 114, D06210, doi:10.1029/2008JD010680, 2009.

Ouimette, J. and Flagan, R.: The extinction coefficient of multicomponent aerosols, Atmos. Environ., 16, 2405–2419, 1982.

Petzold, A., Fiebig, M., Flentje, H., Keil, A., Leiterer, U., Schröder, F., Stifter, A., Wendisch, M., and Wendling, P.: Vertical variability of aerosol properties observed at a continental site during the Lindenberg Aerosol Characterization Experiment (LACE 98), J. Geophys. Res., 107, 8128, doi:10.1029/2001JD001043, 2002.

Pozzer, A., Jöckel, P., Tost, H., Sander, R., Ganzeveld, L., Kerkweg, A., and Lelieveld, J.: Simulating organic species with the global atmospheric chemistry general circulation model ECHAM5/MESSy1: a comparison of model results with observations, Atmos. Chem. Phys., 7, 2527–2550, doi:10.5194/acp-7-2527-2007, 2007.

Pratt, K. A. and Prather, K. A.: Aircraft measurements of vertical profiles of aerosol mixing states, J. Geophys. Res, 115, D11305, doi:10.1029/2009JD013150, 2010.

Price, C. and Rind, D.: A simple lightning parameterization for calculating global lightning distributions, J. Geophys. Res., 97, 9919–9933, 1992.

Pringle, K. J., Tost, H., Message, S., Steil, B., Giannadaki, D., Nenes, A., Fountoukis, C., Stier, P., Vignati, E., and Lelieveld, J.: Description and evaluation of GMXe: a new aerosol submodel for global simulations (v1), Geosci. Model Dev., 3, 391–412, doi:10.5194/gmd-3-391-2010, 2010.

Prospero, J. M.: The Atmospheric Transport of Particles to the Ocean, in: Particle Flux in the Ocean, John Wiley and Sons Ltd., New York, 1996.

Prospero, J. M., Uematsu, M., and Savoie, D. L.: Mineral aerosol transport to the Pacific Ocean, Academic Press, New York, 1989.

Putaud, J.-P., Van Dingenen, R. M., Baltensperger, U., Brueggemann, E., Facchini, M. C., Fuzzi, S., Gehrig, R., Hansson, H. C., Harrison, R. M., Jones, A. M., Laj, P., Maenhaut, W., Mihalopoulos, N., Mueller, K., Palmgren, F., Querol, X., Rodriguez, S., Spindler, G., Ten Brink, H., Tunved, P., Wehner, B., Weingartner, W., Wiedensohler, A., Waehlin, P., and Raes, F.: A European Aerosol Phenomenology: Physical and Chemical Characteristics of Particulate Matter at Kerbside, Urban, Rural and Background Sites in Europe, JRC Scientific and Technical Reports (EUR collection) EUR 20411 EN, Joint Research Center, JRC23835, 2002.

Rayner, N. A., Parker, D. E., Horton, E. B., Folland, C. K., Alexander, L. V., Rowell, D. P., Kent, E. C., and Kaplan, A.: Global analyses of sea surface temperature, sea ice, and night marine air temperature since the late nineteenth century, J. Geophys. Res., 108, 4407, doi:10.1029/2002JD002670, 2003.

Riemer, N., Vogel, H., Vogel, B., and Fiedler, F.: Modeling aerosol on the mesoscale-γ: treatment of soot aerosol and its radiative effects, J. Geophys. Res., 108, 4601, doi:10.1029/2003JD003448, 2003.

Riemer, N., West, M., Zaveri, R. A., and Easter, R. C.: Simulating the evolution of soot mixing state with a particle-resolved aerosol model, J. Geophys. Res., 114, D09202, doi:10.1029/2008JD011073, 2009.

Roeckner, E., Bäuml, G., Bonaventura, L., Brokopf, R., Esch, M., Giorgetta, M., Hagemann, S., Kirchner, I., Kornblueh, L., Manzini, E., Rhodin, A., Schlese, U., Schulzweida, U., and Tompkins, A.: The atmospheric general circulation model ECHAM5: Part 1. Model description, Report 349, Max-Plan-Institut fuer Meteorologie, 2003.

Roeckner, E., Brokopf, R., Esch, M., Giorgetta, M., Hagemann, S., Kornblueh, L., Manzini, E., Schlese, U., and Schulzweida, U.: Sensitivity of simulated climate to horizontal and vertical resolution in the ECHAM5 atmosphere model, J. Climate, 19, 3771–3791, 2006.

Sander, R., Kerkweg, A., Jöckel, P., and Lelieveld, J.: Technical note: The new comprehensive atmospheric chemistry module MECCA, Atmos. Chem. Phys., 5, 445–450, doi:10.5194/acp-5-445-2005, 2005.

Schnaiter, M., Linke, C., Möhler, O., Naumann, K.-H., Saathoff, H., Wagner, R., Schurath, U., and Wehner, B.: Absorption amplification of black carbon internally mixed with secondary organic aerosol, J. Geophys. Res., 110, D19204, doi:10.1029/2005JD006046, 2005.

Schröder, F. B. K., Fiebig, M., and Petzold, A.: Aerosol states in the free troposphere at northern midlatitudes, J. Geophys. Res., 107, 8126, doi:10.1029/2000JD000194, 2002.

Schwarz, J., Gao, R. S., Fahey, D. W., Thomson, D. S., Watts, L. A., Wilson, J. C., Reeves, J. M., Darbeheshti, M., Bamgardner, D. G., Kok, G. L., Chung, S. H., Schulz, M., Hendricks, J., Lauer, A., Kärcher, B., Slowik, J. G., Rosenlof, K. H., Thompson, T. L., Langford, A. O., Loewenstein, M., and Aikin, K. C.: Single-particle measurements of midlatitude black carbon and light-scattering aerosols from the boundary layer to the lower stratosphere, J. Geophys. Res, 111, D16207, doi:10.1029/2006JD007076, 2006.

Schwarz, J. P., Spackman, J., Fahey, D. W., Gao, R. S., Lohmann, U., Stier, P., Watts, L. A., Thomson, D. S., Lack, D. A., Pfister, L., Mahoney, M. J., Baumgardner, D., Wilson, J., and Reeves, J. M.: Coatings and their enhancement of black-carbon light absorption in the tropical atmosphere, J. Geophys. Res., 113, D03203, doi:10.1029/2007JD009042, 2008.

Seland, Ø., Iversen, T., Kirkevåg, A., and Storelvmo, T.: Aerosol-climate interactions in the CAM-Oslo atmospheric GCM and investigation of associated basic shortcomings, Tellus, 60A, 459–491, 2008.

Sheridan, J. S., Brock, C. A., and Wilson, J. C.: Aerosol particles in the upper troposphere and lower stratosphere: Elemental composition and morphology of individual particles in the northern midlatitude, Geophys. Res. Lett., 21, 2587–2590, 1994.

Shiraiwa, M., Kondo, Y., Moteki, N., Takegawa, N., Sahu, L. K., Takami, A., Hatakeyama, S., Yonemura, S., and Blake, D. R.: Radiative impact of mixing state of black carbon aerosol in Asian outflow, J. Geophys. Res., 113, D24210, doi:10.1029/2008JD010546, 2008.

Smith, M. H. and Harrison, N. M.: The sea spray generation func-

tion, J. Aerosol Sci., 29, S189–S190, 1998.

Song, C. H., Maxwell-Meier, K., Weber, R. J., Kapustin, V., and Clarke, A.: Dust composition and mixing state inferred from airborne composition measurements during ACE-Asia C130 Flight #6, Atmos. Environ., 39, 359–369, doi:10.1016/j.atmosenv.2004.08.046, 2005.

Spackman, J. R., Gao, R. S., Schwarz, J. P., Watts, L. A., Fahey, D. W., Pfister, L., and Bui, T. P.: Seasonal variability of black carbon mass in the tropical tropopause layer, Geophys. Res. Lett., doi:10.1029/2010GL046343, in press, 2010.

Stier, P., Feichter, J., Kinne, S., Kloster, S., Vignati, E., Wilson, J., Ganzeveld, L., Tegen, I., Werner, M., Balkanski, Y., Schulz, M., Boucher, O., Minikin, A., and Petzold, A.: The aerosol-climate model ECHAM5-HAM, Atmos. Chem. Phys., 5, 1125–1156, doi:10.5194/acp-5-1125-2005, 2005.

Sullivan, R. C., Guazzotti, S. A., Sodeman, D. A., and Prather, K. A.: Direct observations of the atmospheric processing of Asian mineral dust, Atmos. Chem. Phys., 7, 1213–1236, doi:10.5194/acp-7-1213-2007, 2007.

Sullivan, R. C., Moore, M. J. K., Petters, M. D., Kreidenweis, S. M., Roberts, G. C., and Prather, K. A.: Effect of chemical mixing state on the hygroscopicity and cloud nucleation properties of calcium mineral dust particles, Atmos. Chem. Phys., 9, 3303–3316, doi:10.5194/acp-9-3303-2009, 2009.

Takemura, T., Okamoto, H., Maruyama, Y., Numaguti, A., Higurashi, A., and Nakajima, T.: Global three-dimensional simulation of aerosol optical thickness distribution of various origins, J. Geophys. Res., 105, 17853–17873, 2000.

Textor, C., Schulz, M., Guibert, S., Kinne, S., Balkanski, Y., Bauer, S., Berntsen, T., Berglen, T., Boucher, O., Chin, M., Dentener, F., Diehl, T., Feichter, J., Fillmore, D., Ginoux, P., Gong, S., Grini, A., Hendricks, J., Horowitz, L., Huang, P., Isaksen, I. S. A., Iversen, T., Kloster, S., Koch, D., Kirkevåg, A., Kristjansson, J. E., Krol, M., Lauer, A., Lamarque, J. F., Liu, X., Montanaro, V., Myhre, G., Penner, J. E., Pitari, G., Reddy, M. S., Seland, Ø., Stier, P., Takemura, T., and Tie, X.: The effect of harmonized emissions on aerosol properties in global models - an AeroCom experiment, Atmos. Chem. Phys., 7, 4489–4501, doi:10.5194/acp-7-4489-2007, 2007.

Tiedtke, M.: A comprehensive mass flux scheme for cumulus parameterization in large-scale models, Mon. Weather Rev., 117, 1779–1800, 1989.

Tost, H., Jöckel, P., Kerkweg, A., Sander, R., and Lelieveld, J.: Technical note: A new comprehensive SCAVenging submodel for global atmospheric chemistry modelling, Atmos. Chem. Phys., 6, 565–574, doi:10.5194/acp-6-565-2006, 2006a.

Tost, H., Jöckel, P., and Lelieveld, J.: Influence of different convection parameterisations in a GCM, Atmos. Chem. Phys., 6, 5475–5493, doi:10.5194/acp-6-5475-2006, 2006b.

Tost, H., Jöckel, P., Kerkweg, A., Pozzer, A., Sander, R., and Lelieveld, J.: Global cloud and precipitation chemistry and wet deposition: tropospheric model simulations with ECHAM5/MESSy1, Atmos. Chem. Phys., 7, 2733–2757, doi:10.5194/acp-7-2733-2007, 2007.

Vanderzalm, J. L., Hooper, M. A., Ryan, B., Maenhaut, W., Martin, P., Rayment, P. R., and Hooper, B. M.: Impact of seasonal biomass burning on air quality in the "Top" End of regional Northern Australia, Clean Air and Environmental Quality, 37, 28–34, 2003.

Vehkamäki, H., Kulmala, M., Napari, I., Lehtinen, K. E. J., Timmreck, C., Noppel, M., and Laaksonen, A.: An improved parameterization for sulfuric acid-water nucleation rates for tropospheric and stratospheric conditions, J. Geophys. Res., 107, 4622, doi:10.1029/2002JD002184, 2002.

Vignati and Wilson: M7: An efficient size-resolved aerosol microphysical module for large-scale aerosol transport models, J. Geophys. Res., 109, D22202, doi:10.1029/2003JD004485, 2004.

Wang, M., Penner, J. E., and Liu, X.: Coupled IMPACT aerosol and NCAR CAM3 model: Evaluation of predicted aerosol number and size distribution, J. Geophys. Res., 114, D06302, doi:10.1029/2008JD010459, 2009.

Weingartner, E., Burtscher, H., and Baltensperger, H.: Hygroscopic properties of carbon and diesel soot particles, Atmos. Environ., 31, 2311–2327, 1997.

Weingartner, E., Saathoff, H., Streit, N., Lavanchy, V., Schnaiter, M., Matter, U., and Baltensperger, U.: Hygroscopic behaviour of soot particles coated with oxidation products of α-pinene, J. Aerosol Sci., 31, S987–S988, 2000.

Weinzierl, B., Petzold, A., Esselborn, M., Wirth, M., Rasp, K., Kandler, K., Schütz, L., Koepke, P., and Fiebig, M.: Airborne measurements of dust layer properties, particle size distribution and mixing state of Saharan dust during SAMUM 2006, Tellus B, 61, 96–117, 2009.

Whitby, E. and McMurry, P.: Modal Aerosol Dynamics Modelling, Aerosol Sci. Tech., 27, 673–688, 1997.

Whitby, E. R., McMurray, P., Shankar, U., and Binkowski, F.: Modal Aerosol Dynamics Modeling, Tech. Rep. 600/3-91/020, Atmospheric Research and Exposure Assess. Lab., US Environmental Protection Agency, Research Triangle Park, available as NTIS PB91-161729/AS, 1991.

Zuberi, B., Johnson, K. S., Aleks, G. K., Molina, L. T., Molina, M. J., and Laskin, A.: Hydrophilic properties of aged soot, Geophys. Res. Lett., 32, L01807, doi:10.1029/2004GL021496, 2005.